RSC Advances

PAPER

View Article Online
View Journal | View Issue



Cite this: *RSC Adv.*, 2022, **12**, 11164

# Diverse and efficient catalytic applications of new cockscomb flower-like $Fe_3O_4$@$SiO_2$@KCC-1@MPTMS@$Cu^{II}$ mesoporous nanocomposite in the environmentally benign reduction and reductive acetylation of nitroarenes and one-pot synthesis of some coumarin compounds†

Morteza Hasanpour Galehban, Behzad Zeynizadeh and Hossein Mousavi *

In this research, $Fe_3O_4$@$SiO_2$@KCC-1@MPTMS@$Cu^{II}$ as a new cockscomb flower-like mesoporous nanocomposite was prepared and characterized by various techniques including Fourier transform infrared (FT-IR) spectroscopy, powder X-ray diffraction (PXRD), scanning electron microscopy (SEM), transmission electron microscopy (TEM), SEM-based energy-dispersive X-ray (EDX) spectroscopy, inductively coupled plasma-optical emission spectrometry (ICP-OES), thermogravimetric analysis/differential thermal analysis (TGA/DTA), vibrating sample magnetometry (VSM), UV-Vis spectroscopy, and Brunauer–Emmett–Teller (BET) and Barrett–Joyner–Halenda (BJH) analyses. The as-prepared $Fe_3O_4$@$SiO_2$@KCC-1@MPTMS@$Cu^{II}$ mesoporous nanocomposite exhibited satisfactory catalytic activity in the reduction and reductive acetylation of nitroarenes in a water medium and solvent-free one-pot synthesis of some coumarin compounds including 3,3′-(arylmethylene)bis(4-hydroxy-2*H*-chromen-2-ones) (namely, bis-coumarins) (**3a–n**) and 2-amino-4-aryl-7,7-dimethyl-5-oxo-5,6,7,8-tetrahydro-4*H*-chromene-3-carbonitriles (**6a–n**) along with acceptable turnover numbers (TONs) and turnover frequencies (TOFs). Furthermore, the mentioned $Cu^{II}$-containing mesoporous nanocatalyst was conveniently recovered by a magnet from reaction environments and reused for at least seven cycles without any significant loss in activity, which confirms its good stability.

Received 1st December 2021
Accepted 17th January 2022

DOI: 10.1039/d1ra08763k

rsc.li/rsc-advances



## 1. Introduction

From the green chemistry point of view, designing chemical reactions considering all their environmental aspects is very precious. To this purpose, twelve main protocols with many sub-branches have been introduced, which guide and assist chemistry scientists, particularly synthetic chemists, in designing efficient and environmentally benign chemical strategies.[1] Catalysis is one of the most significant parts of green chemistry protocols, and plays a unique role in a wide range of organic transformations.[2] For the sake of the demands of sustainable development and green chemistry, the use of heterogeneous catalytic systems instead of traditional homogeneous ones has received increasing attention.[3] In recent years and among heterogeneous catalysts, magnetic core–shell-type nanostructures have received tremendous attention and have significantly grown.[4] In these types, magnetic iron oxide nanoparticles ($Fe_3O_4$ NPs) have been widely used as the central part of the core in the core–shell system due to their fantastic properties, especially satisfactory and powerful magnetic behaviors that facilitate the separation of the multi-layer-containing core–shell-sort catalytic system from the reaction pot using a simple magnet. Another important element for the construction of suitable core–shell-type nanocatalysts is supporting easily functionalizable surfaces. In this regard, silica-based mesoporous materials such as Santa Barbara Amorphous-15 (SBA-15), Mobil Composition of Matter No. 41 and 48 (MCM-41 and MCM-48), hollow mesoporous silica (HMS), and KAUST Catalysis Center (KCC-1) have emerged as some of the most important platforms, for which in recent decades, the scientific community has witnessed a notable increase in the design and development. Among various types of mesoporous silica-based materials, dendritic fibrous nano-silica KCC-1 with three-dimensional (3D) center-radial wrinkle channels and hierarchical pores has unique structural characteristics including open-pore nanochannels, highly accessible internal spaces with a high surface area typically > 700 $m^2\ g^{-1}$,

*Department of Organic Chemistry, Faculty of Chemistry, Urmia University, Urmia, Iran. E-mail: 1hossein.mousavi@gmail.com*

† Electronic supplementary information (ESI) available. See DOI: 10.1039/d1ra08763k

large pore volumes, ease of surface modification, low density, satisfactory stability, low toxicity, and good biocompatibility compared with conventional mesoporous materials.[5] During the last decade and after the first report for the hydrothermal preparation of KCC-1 by Polshettiwar and co-workers in 2010,[6] considerable attention and experience rapidly developed in terms of synthetic techniques, formation mechanisms, functionalization approaches, and application fields upon mentioned dendritic fibrous nanosilica-based materials. Catalysis is one of the most substantial areas that KCC-1 has a unique effect on it. The literature survey shows that the use of KCC-1-containing catalytic systems in various organic transformations has been increasing day by day.[7]

Nitroarenes, especially 4-nitrophenol (4-NP), and related compounds are known as notorious organic pollutants present in industrial and agriculture wastewaters, unfortunately.[8] In this regard and due to the increasing global environmental concerns, the transformation of these hazardous compounds to valuable organic molecules such as arylamines (*via* a green reduction process) and arylacetamides (*via* a direct one-pot reductive acetylation strategy) is desirable in the organic and industrial chemistry community. Till date, various catalytic methods have been reported for the mentioned chemical transformations. However, numerous efficient catalytic procedures have been widely used for the reduction and reductive acetylation of nitroarenes but introducing new, stable, non-hazardous, cost-effective, easily accessible active site(s), and efficient catalytic systems that are capable of carrying out these organic reactions in green solvents are still needed. Without a doubt, among green solvents, water is the best choice in every way because it is readily available, very cheap, safe, non-flammable, and so on.[9]

Coumarins and related compounds (namely, coumarin-fused or coumarin-linked heterocycles) are an outstanding

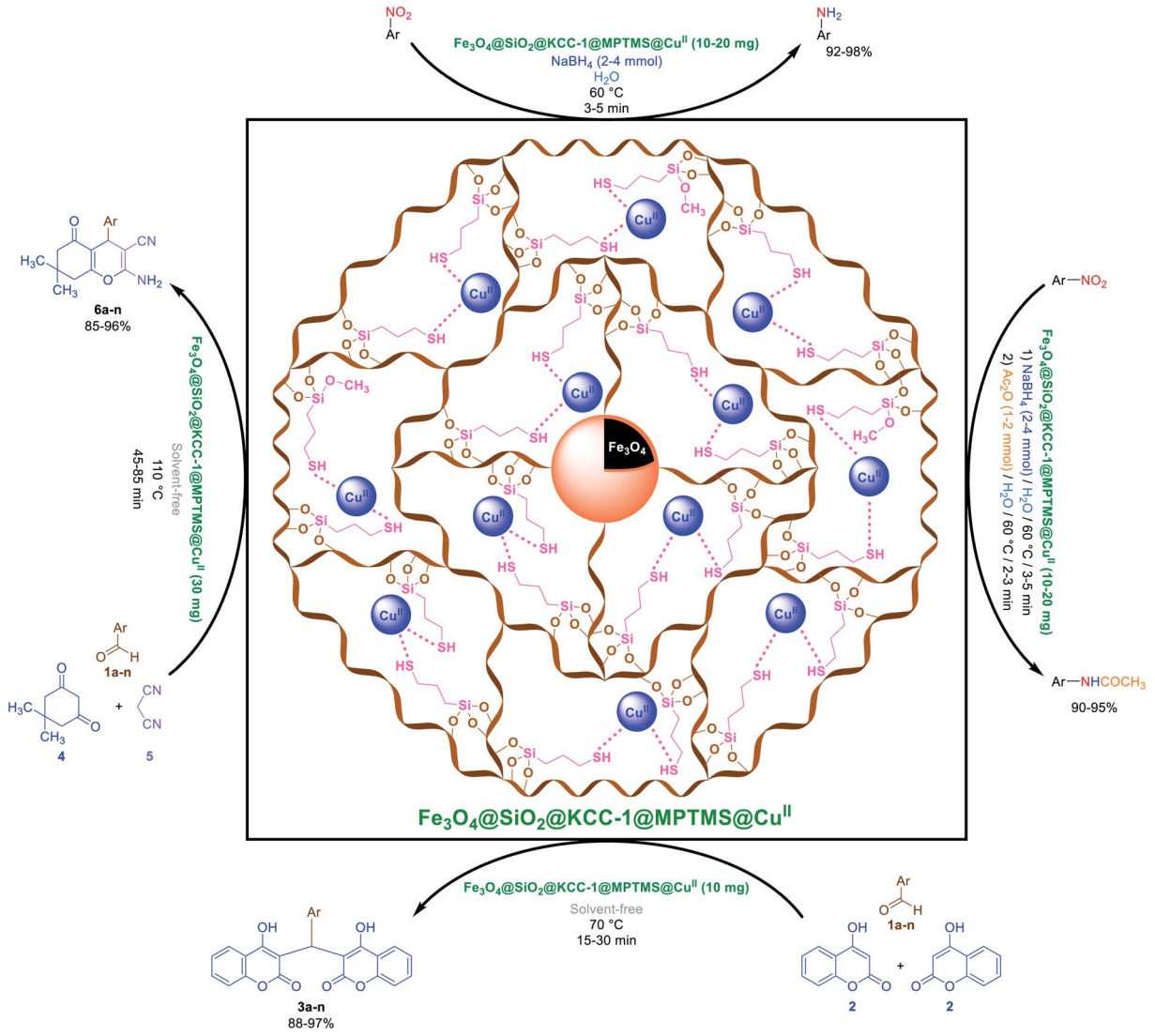


Fig. 1 Catalytic applications of the cockscomb flower-like $Fe_3O_4$@$SiO_2$@KCC-1@MPTMS@$Cu^{II}$ mesoporous nanocomposite in the reduction and reductive acetylation of nitroarenes in water and solvent-free one-pot synthesis of some coumarin compounds.

family of oxygen-containing fused heterocyclic frameworks. These scaffolds have diverse biological properties including anticancer,[10] antioxidant,[11] antidepressant,[12] antimicrobial,[13] anti-nociceptive,[14] anti-asthmatic,[15] anti-inflammatory,[16] antipyretic,[17] antileishmanial,[18] anti-coagulant,[19] anti-tubercular,[20] antiviral,[21] antibacterial,[22] antifungal,[23] antimalarial,[24] antidiabetic,[25] anti-hepatitis C virus,[26] anti-HIV,[27] anti-proliferative,[28] antiplatelet,[29] and antiplasmodial[30] activities. They are also well-known inhibitors of urease,[31] acetylcholinesterase (AChE) and butyrylcholinesterase (BChE),[32] cyclooxygenase (COX),[33] lipoxygenase (LOX),[34] monoamine oxidases A and B (MAO-A and MAO-B),[35] tubulin polymerization,[36] carbonic anhydrase,[37] α-glucosidase,[38] inositol-requiring enzyme 1 (IRE-1) RNase,[39] mitochondria-targeting antitumor STAT3,[40] selective cyclin-dependent kinase 9 (CDK9),[41] selective aldehyde dehydrogenase 1A1,[42] coagulation factor XIIa (FXIIa),[43] casein kinase 2 (CK2),[44] steroid sulfatase (STS),[45] chitin synthase (CHS),[46] *etc.* These heterocyclic scaffolds have antagonistic behavior against chemokine-like factor 1 (CKLF1),[47] G-protein-coupled receptor 35 (GPR35),[48] orphan G-protein-coupled receptor 55 (GPR55),[49] $A_3$ adenosine receptor,[50] and many others. According to the various and significant biological attributes of the coumarin derivatives, introducing powerful and simple synthetic methods for the preparation of such valuable heterocyclic scaffolds along with respect to green chemistry protocols are undoubtedly precious. One-pot multi-component reactions (MCRs) could be a very suitable strategy for this purpose. These reactions are fast,

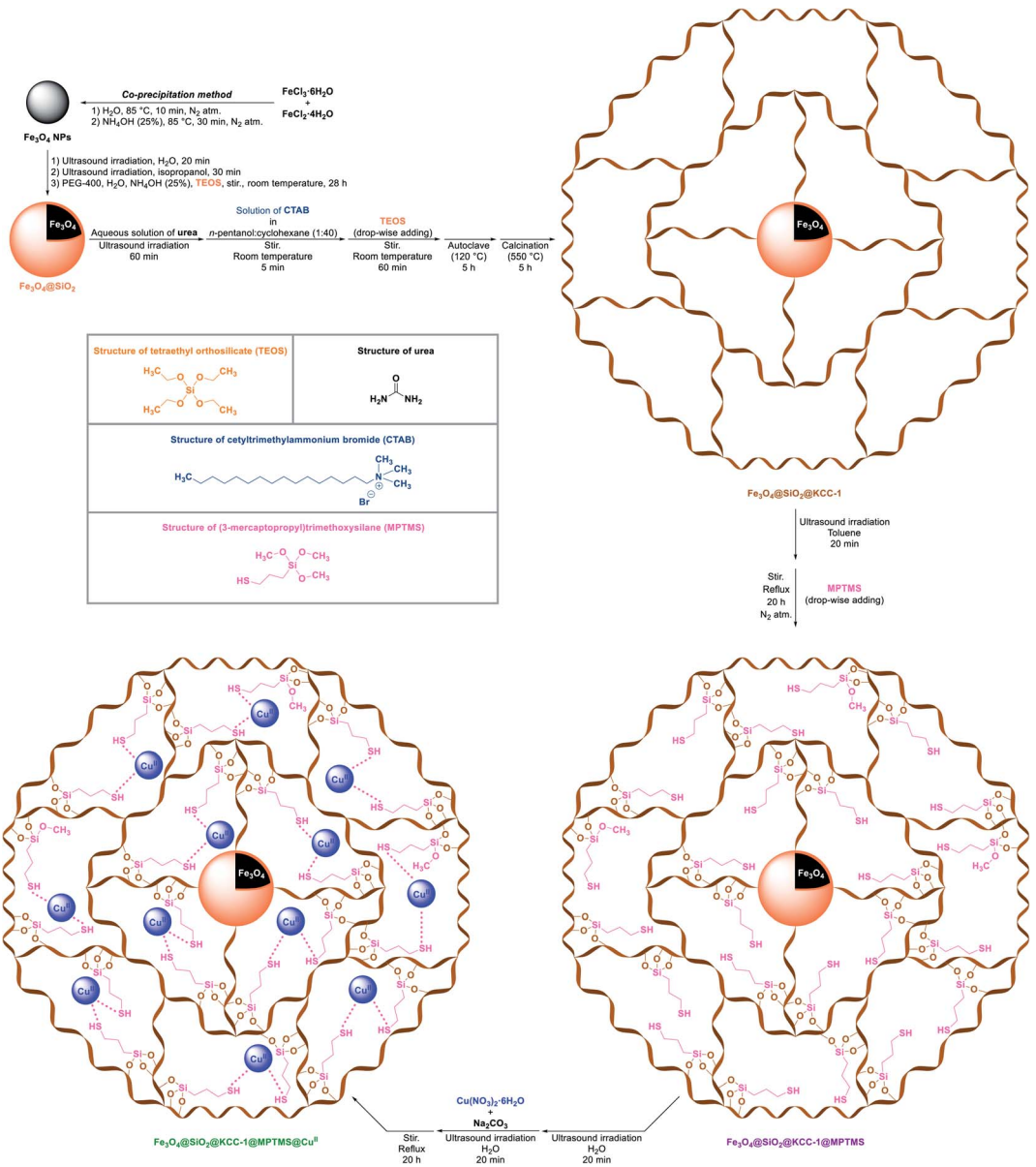


Scheme 1 Preparation of the cockscomb flower-like $Fe_3O_4$@$SiO_2$@KCC-1@MPTMS@$Cu^{II}$ mesoporous nanocomposite.

convenient, atom-economic, safe, effective, and more economic than the classical multi-step synthetic manners.[51]

Herein, in continuation of our research program in organic synthesis[52] and new catalytic systems design, we report a multi-step strategy for the preparation of a new magnetic core–shell-type cockscomb flower-like $Fe_3O_4$@$SiO_2$@KCC-1@MPTMS@$Cu^{II}$ mesoporous nanocomposite as an efficient, recoverable, reusable, and stable nano-based catalytic system in the environmentally benign reduction and reductive acetylation of aromatic nitro compounds in water and solvent-free one-pot synthesis of some coumarin compounds including 3,3′-(arylmethylene)bis(4-hydroxy-2*H*-chromen-2-ones) (namely, bis-coumarins) (**3a–n**) and 2-amino-4-aryl-7,7-dimethyl-5-oxo-5,6,7,8-tetrahydro-4*H*-chromene-3-carbonitriles (**6a–n**) (Fig. 1).

## 2. Results and discussion

### 2.1 Preparation and characterization of the $Fe_3O_4$@$SiO_2$@KCC-1@MPTMS@$Cu^{II}$ mesoporous nanocomposite

Initially, we designed and implemented a five-step synthetic strategy for the preparation of the cockscomb flower-like $Fe_3O_4$@$SiO_2$@KCC-1@MPTMS@$Cu^{II}$ nanocomposite. First of all, and as shown in Scheme 1, the $Fe_3O_4$ nanoparticles (NPs) were prepared by a convenient and well-known chemical co-precipitation method of $FeCl_3 \cdot 6H_2O$ and $FeCl_2 \cdot 4H_2O$ in an aqueous ammonia solution under a nitrogen gas atmosphere. In the next step, the layering of $SiO_2$ on the magnetic $Fe_3O_4$ NPs, which caused the formation of the $Fe_3O_4$@$SiO_2$ core–shell structure, was carried out using tetraethyl orthosilicate (TEOS) at room temperature. In the third stage, the dendritic silica were grown around the surface of the $Fe_3O_4$@$SiO_2$ nanocomposite using urea, cetyltrimethylammonium bromide (CTAB), and TEOS, and subsequently the whole mixture was heated (120 °C) in an autoclave and then calcined at 500 °C. After preparation of the magnetic $Fe_3O_4$@$SiO_2$@KCC-1 nanocomposite, functionalization of the mentioned dendritic silica section was accomplished with (3-mercaptopropyl)trimethoxysilane (MPTMS), which afforded the fibrous $Fe_3O_4$@$SiO_2$@KCC-1@MPTMS. In the final step, the immobilization of the copper$^{II}$ species on the dendritic $Fe_3O_4$@$SiO_2$@KCC-1@MPTMS system yielded the cockscomb flower-like $Fe_3O_4$@$SiO_2$@KCC-1@MPTMS@$Cu^{II}$ mesoporous nanocomposite using copper$^{II}$ nitrate hexahydrate ($Cu(NO_3)_2 \cdot 6H_2O$) and sodium carbonate ($Na_2CO_3$) in a water medium. After building the $Fe_3O_4$@$SiO_2$@KCC-1@MPTMS@$Cu^{II}$ core–shell-type nanosystem, the structure of the as-prepared nanocomposite was elucidated by FT-IR, PXRD, SEM, TEM, SEM-based EDX, ICP-OES, TGA/DTA, VSM, UV-Vis, and BET and BJH analyses.

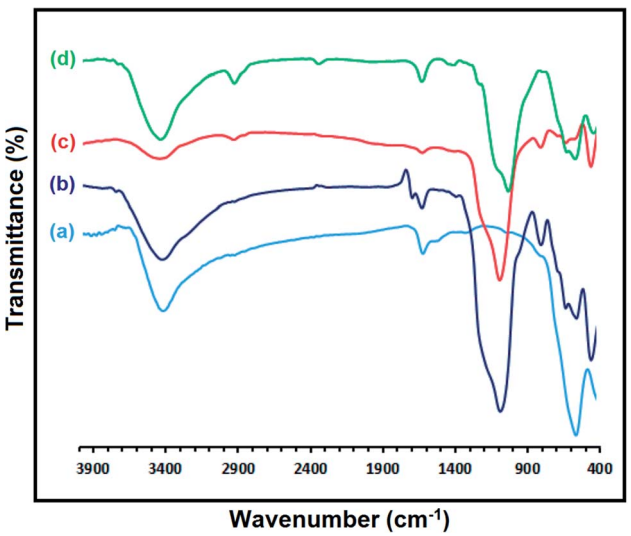


Fig. 2 FT-IR spectra of the (a) $Fe_3O_4$, (b) $Fe_3O_4$@$SiO_2$@KCC-1, (c) $Fe_3O_4$@$SiO_2$@KCC-1@MPTMS, and (d) $Fe_3O_4$@$SiO_2$@KCC-1@MPTMS@$Cu^{II}$ nanosystems.

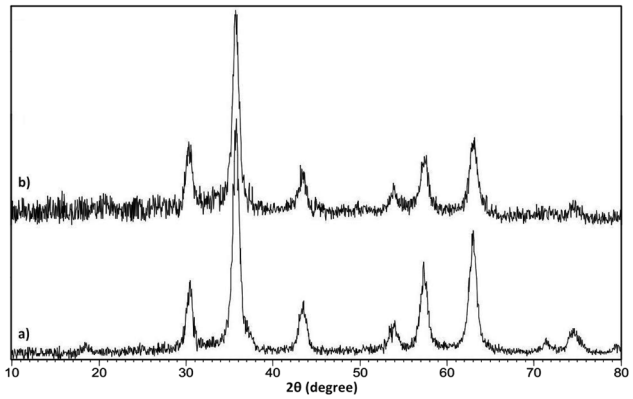


Fig. 3 PXRD patterns of the (a) $Fe_3O_4$ and (b) $Fe_3O_4$@$SiO_2$@KCC-1@MPTMS@$Cu^{II}$ nanostructures.

The FT-IR spectroscopy analysis was used to elucidate the functional groups that exist in the structure of $Fe_3O_4$, $Fe_3O_4$@$SiO_2$@KCC-1, $Fe_3O_4$@$SiO_2$@KCC-1@MPTMS, and $Fe_3O_4$@$SiO_2$@KCC-1@MPTMS@$Cu^{II}$. In the FT-IR spectrum of the bare $Fe_3O_4$ NPs (Fig. 2a), a strong absorption peak appeared at 575 $cm^{-1}$ attributed to the vibration of Fe–O bonds and absorption peaks also appeared at 1625 $cm^{-1}$ and 3400 $cm^{-1}$ due to the O–H deforming and stretching vibrations of OH groups or adsorbed water on the $Fe_3O_4$ NPs surface, respectively. As shown in Fig. 2 (curves b and c), in the FT-IR spectrum of the $Fe_3O_4$@$SiO_2$@KCC-1 and $Fe_3O_4$@$SiO_2$@KCC-1@MPTMS, the absorption peaks appear at 808 $cm^{-1}$ and 1091 $cm^{-1}$ (strong), which are ascribed to the symmetric and asymmetric stretching vibrations of Si–O–Si, and there exists a peak at 2929 $cm^{-1}$ assigned to the C–H stretching vibration of the aliphatic moiety in MPTMS. After adding copper$^{II}$ and forming the $Fe_3O_4$@$SiO_2$@KCC-1@MPTMS@$Cu^{II}$ nanocomposite, all the mentioned distinguished peaks existed and are visible (Fig. 2d).

The phase purity and crystallinity character of the alone $Fe_3O_4$ NPs and as-prepared $Fe_3O_4$@$SiO_2$@KCC-1@MPTMS@$Cu^{II}$ nanocomposite were studied by PXRD analysis. The PXRD pattern of the $Fe_3O_4$ NPs (Fig. 3a) shows the reflection planes at nine diffraction peaks at (111), (220), (311), (400), (422), (511), (440), (620), and (553), which are indexed to

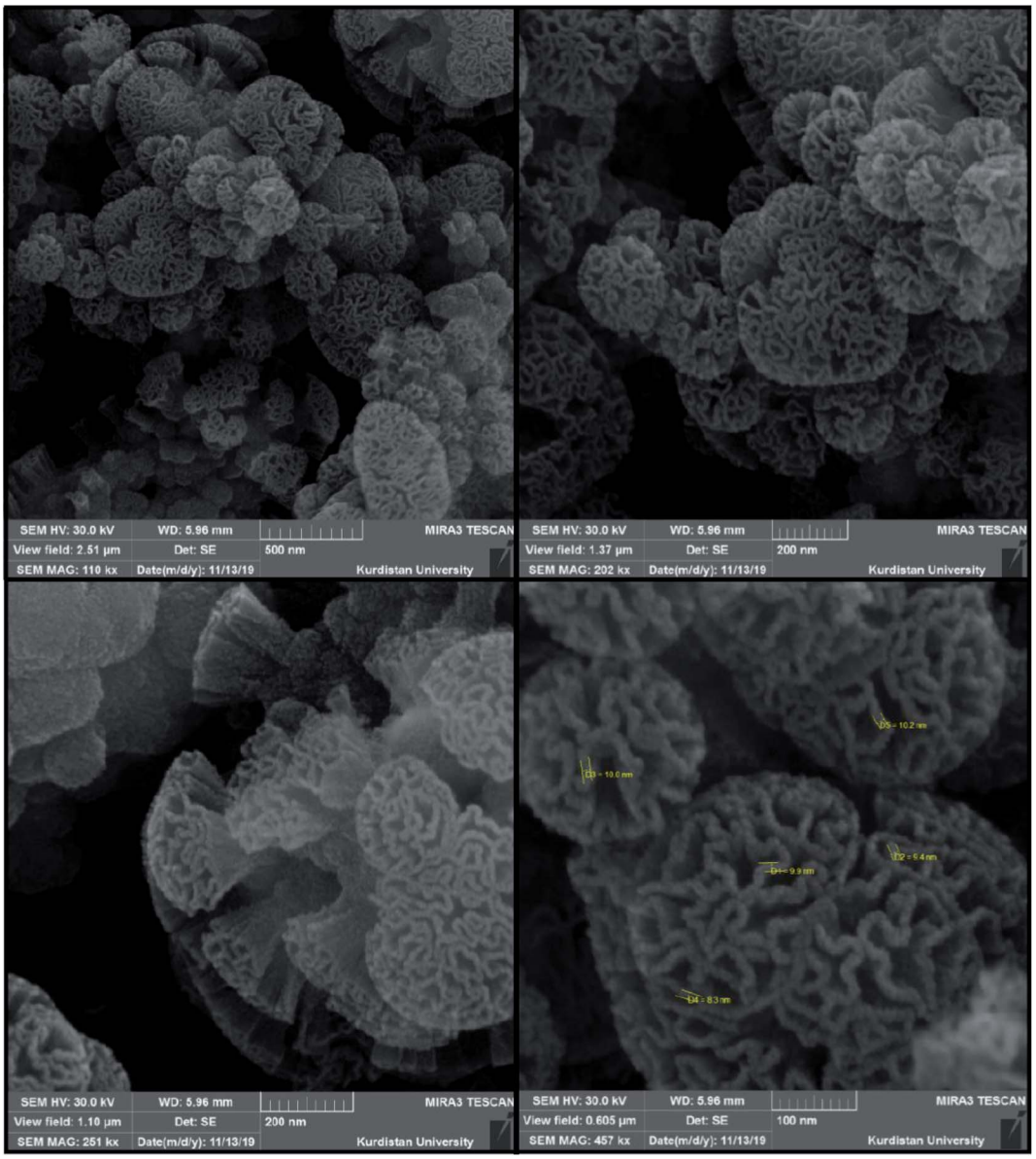


Fig. 4 SEM images of the cockscomb flower-like $Fe_3O_4$@$SiO_2$@KCC-1@MPTMS@$Cu^{II}$ nanocomposite.

the cubic spinel phase of $Fe_3O_4$, appeared and matched well with Joint Committee on Powder Diffraction Standards (JCPDS) card no. 65-3107. Comparing the PXRD patterns of the $Fe_3O_4$@$SiO_2$@KCC-1@MPTMS@$Cu^{II}$ nanocomposite (Fig. 3b) and alone $Fe_3O_4$ NPs (Fig. 3a) shows that both patterns have the same signal position and crystallinity character. The wide and weak peak at around $2\theta = 20$–$23^\circ$ is related to the amorphous silica and proved the effective coating of the silica on the $Fe_3O_4$ core. Notably, in the PXRD pattern of the $Fe_3O_4$@$SiO_2$@KCC-1@MPTMS@$Cu^{II}$ nanocomposite (Fig. 3b), the index reflection peaks of the corresponding $Cu^{II}$ species (JCPDS card no. 00-004-0836) were not clearly recognizable due to the overlapping of its signals with $Fe_3O_4$.

SEM and TEM techniques were utilized for the exploration of the $Fe_3O_4$@$SiO_2$@KCC-1@MPTMS@$Cu^{II}$ nanocomposite morphology and size distribution. As shown in SEM images (Fig. 4), the as-prepared nanocomposite has an approximately cockscomb flower-like shape along with three-dimensional center-radial wrinkle channels and hierarchical pores. The SEM images also show that the thickness of wrinkled fibers is around eight to ten nanometers. Notably, this type of open hierarchical channel structure is more appropriate for extreme inter-collisions of the chemical reactants, and facilitates the accessibility of the active sites of the catalytic system. Besides, the TEM images (Fig. 5) reveal identical, well-defined, and ordered dendritic morphology of the as-prepared $Fe_3O_4$@$SiO_2$@KCC-1@MPTMS@$Cu^{II}$, which comes out from the center of the mentioned nanocomposite and is distributed uniformly in all directions.

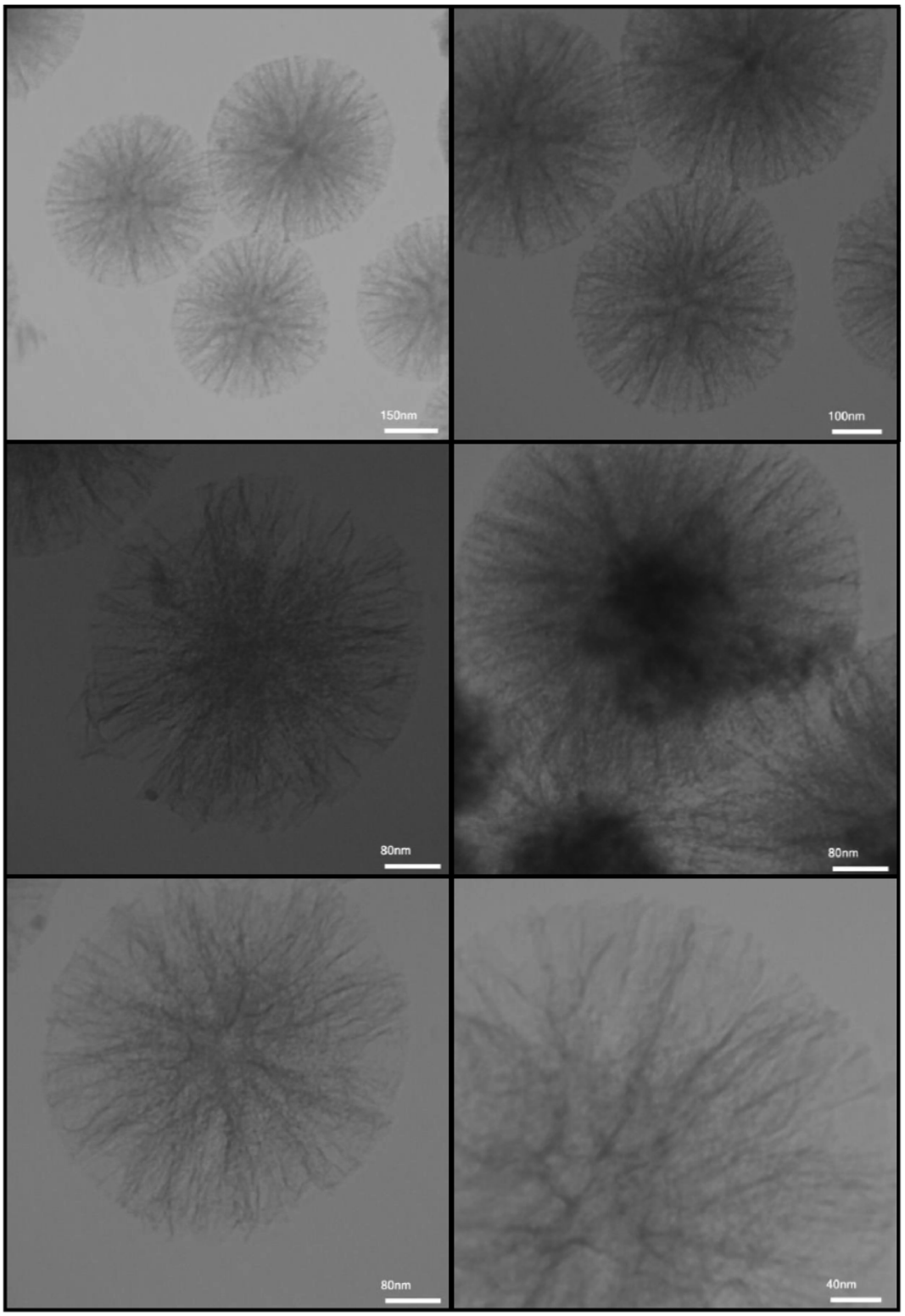


Fig. 5 TEM images of the dendritic $Fe_3O_4$@$SiO_2$@KCC-1@MPTMS@$Cu^{II}$ nanocomposite.

The elemental composition of the dendritic $Cu^{II}$-containing nanocomposite was determined by SEM-based EDX spectroscopy analysis. As shown in Fig. 6, the EDX spectrum shows that in the structure of the mentioned nanocomposite system, the elements of Fe, O, Si, C, Cu, and S existed. Furthermore, using ICP-OES, the actual and exact amounts of the Cu and S species in the $Fe_3O_4$@$SiO_2$@KCC-1@MPTMS@$Cu^{II}$ core–shell-type system were determined to be 14.1% and 1.4%, respectively.

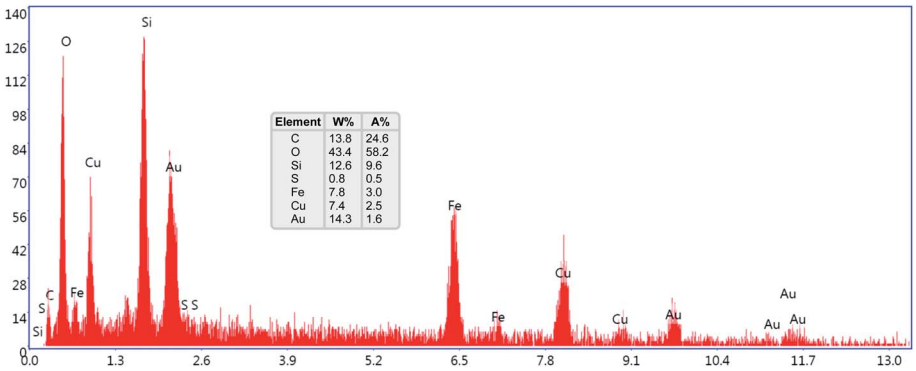


Fig. 6 SEM-based EDX spectrum of the $Fe_3O_4$@$SiO_2$@KCC-1@MPTMS@$Cu^{II}$ nanocomposite.

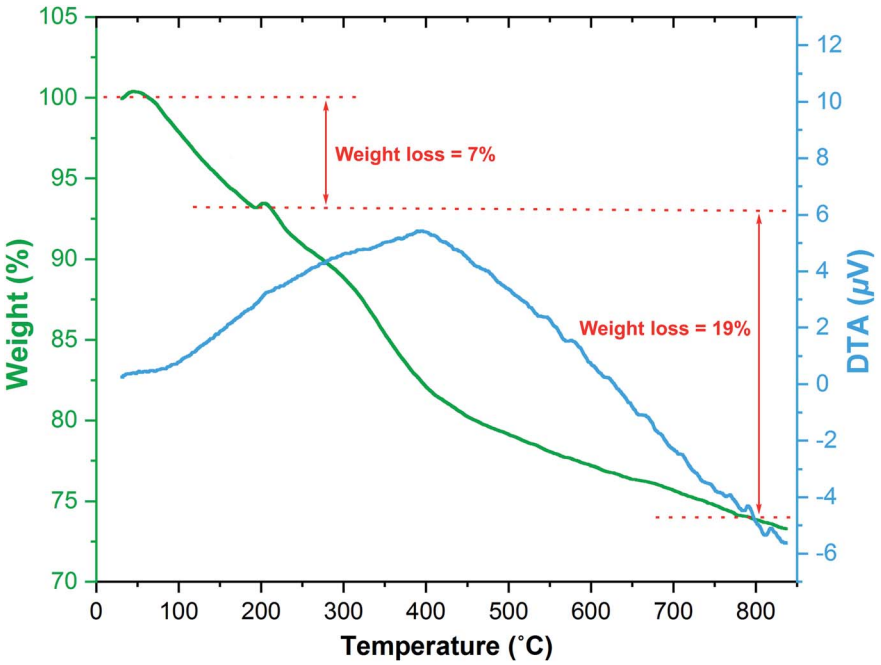


Fig. 7 TGA/DTA diagram of the $Fe_3O_4$@$SiO_2$@KCC-1@MPTMS@$Cu^{II}$ nanocomposite.

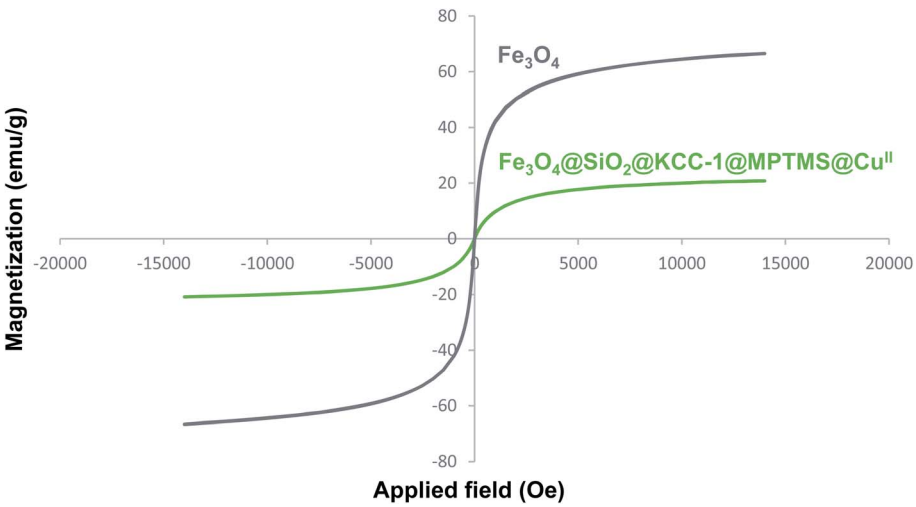


Fig. 8 VSM diagram of the $Fe_3O_4$ NPs and $Fe_3O_4$@$SiO_2$@KCC-1@MPTMS@$Cu^{II}$ nanocomposite.

The thermal stability of the as-prepared dendritic mesoporous $Fe_3O_4$@$SiO_2$@KCC-1@MPTMS@$Cu^{II}$ catalytic system was detected by TGA/DTA in a nitrogen atmosphere (Fig. 7). The first weight loss (around 7%) was observed at temperatures ranging from 60 °C to 200 °C, which could be assigned to trapped solvents (which were applied in the mentioned nanocomposite preparation steps) and adsorbed free water molecules. Moreover, weight losses (around 19%) that occurred in multi-stages between 200 °C and approximately 800 °C belong to the destruction of organic and silicate moieties.

The magnetic property and value of the alone $Fe_3O_4$ NPs and as-prepared $Fe_3O_4$@$SiO_2$@KCC-1@MPTMS@$Cu^{II}$ catalytic system were studied by VSM analysis. As shown in Fig. 8, the saturation magnetization ($M_s$) values of the bare $Fe_3O_4$ NPs and as-prepared dendritic $Cu^{II}$-containing catalyst are respectively 61.62 emu $g^{-1}$ and 17.78 emu $g^{-1}$. The $M_s$ values demonstrate that *via* covering the surface of the $Fe_3O_4$ core with the layering of the amorphous and dendritic silica and then adding diamagnetic copper species to the $Fe_3O_4$@$SiO_2$@KCC-1@MPTMS, the magnetization value of the $Fe_3O_4$@$SiO_2$@KCC-1@MPTMS@$Cu^{II}$ nanocomposite was intensively reduced compared with the bare $Fe_3O_4$ NPs.

Determination of the exact form of the copper species in the structure of the as-prepared catalytic system was performed using the UV-Vis spectroscopy technique. In this context, UV-Vis spectra of the constructed dendritic nanocomposite system with different copper sources including $copper^{II}$ nitrate hexahydrate ($Cu(NO_3)_2 \cdot 6H_2O$), $copper^{I}$ oxide ($Cu_2O$), and $Cu^0$ were recorded (Fig. 9). The results indicated that the as-prepared cockscomb flower-like dendritic nanocomposite in the present work derived from the source of $Cu(NO_3)_2 \cdot 6H_2O$ (*viz.* $Cu^{II}$) exhibited a broad absorption peak around 570–1100 nm. Notably, the constructed nanocomposite by the origins of $Cu_2O$ and $Cu^0$ did not show any absorption peaks. Based on this explanation, the presence of $Cu^{II}$ species in the mentioned nanocomposite system is confirmed.

To determine the specific surface area and surface porosity in the as-prepared dendritic nanocomposite system, the nitrogen ($N_2$) gas adsorption–desorption analysis was performed. Fig. 10 shows the $N_2$ adsorption–desorption profile for the

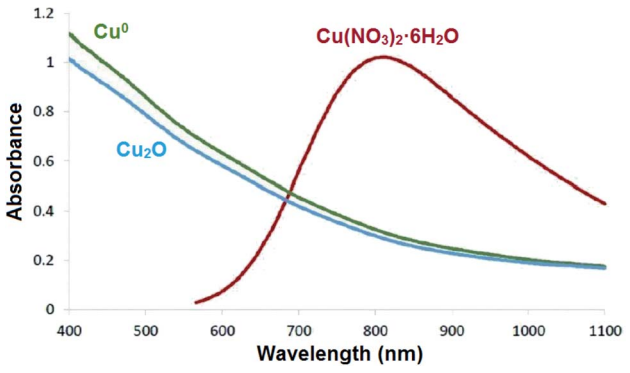


Fig. 9 UV-Vis spectra of the nanocomposite derived from the sources of $Cu(NO_3)_2 \cdot 6H_2O$, $Cu_2O$, and $Cu^0$.

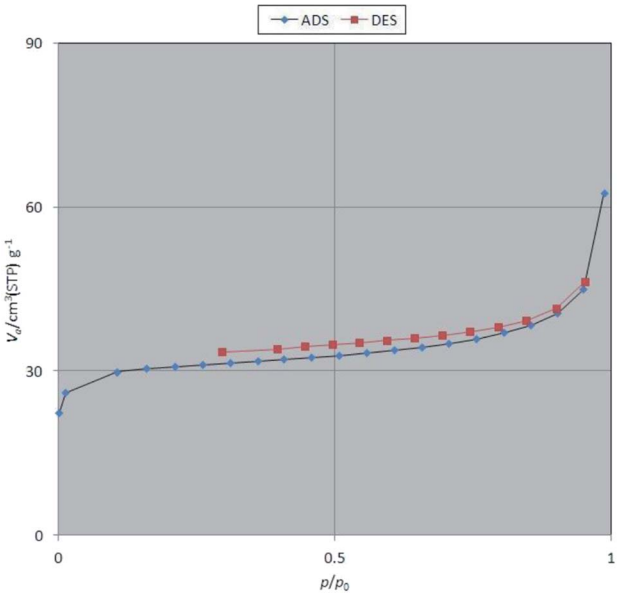


Fig. 10 Nitrogen ($N_2$) gas adsorption–desorption profile of the as-prepared $Fe_3O_4$@$SiO_2$@KCC-1@MPTMS@$Cu^{II}$ mesoporous nanocomposite.

$Fe_3O_4$@$SiO_2$@KCC-1@MPTMS@$Cu^{II}$ nanocomposite. Based on the Brunauer–Deming–Deming–Teller (BDDT) and International Union of Pure and Applied Chemistry (IUPAC) classifications, the shape of the isotherm is closer to the isotherm of type IV with a $H_3$-type hysteresis loop. It is worthy to note that this type of isotherm is a characteristic of mesoporous materials. The specific surface area, pore volume value, and average pore diameter of the as-synthesized mesoporous nanocomposite are 116.13 $m^2$ $g^{-1}$, 26.681 $cm^3$ $g^{-1}$, and 3.331 nm, respectively.

## 2.2 Catalytic applications of the cockscomb flower-like $Fe_3O_4$@$SiO_2$@KCC-1@MPTMS@$Cu^{II}$ mesoporous nanocomposite

**2.2.1 Reduction and one-pot reductive acetylation of nitroarenes.** In the beginning, the catalytic application of the as-prepared magnetic cockscomb flower-like $Fe_3O_4$@$SiO_2$@KCC-1@MPTMS@$Cu^{II}$ mesoporous nanocomposite was investigated upon reduction of nitroarenes, which were converted into the corresponding arylamines using sodium borohydride ($NaBH_4$) as a mild reducing agent. To this purpose, we selected nitrobenzene ($PhNO_2$) as a simplistic aromatic nitro compound for this study. In the first experiment, the conversion of $PhNO_2$ to aniline ($PhNH_2$) using 2 mmol of $NaBH_4$ in the presence of 10 mg of the as-prepared $Fe_3O_4$@$SiO_2$@KCC-1@MPTMS@$Cu^{II}$ catalyst in the water solvent at 60 °C after five minutes was 100% (Table 1, entry 1). The increasing amount of the aforesaid $Cu^{II}$-containing nanocatalyst from 10 mg to 20 mg had no positive effect on the reaction process (Table 1, entry 2). Moreover, the conversion rate of this transformation when carried out in common organic solvents (including $CH_3OH$, $CH_3CH_2OH$, $CH_3CN$, *n*-hexane, and $CH_2Cl_2$) was utterly unsatisfactory (Table 1, entries 3–7). After the optimization steps, the catalytic

Table 1 Optimization experiments for the reduction of $PhNO_2$ to $PhNH_2$ with $NaBH_4$ catalyzed by the $Fe_3O_4$@$SiO_2$@KCC-1@MPTMS@$Cu^{II}$ nanocomposite

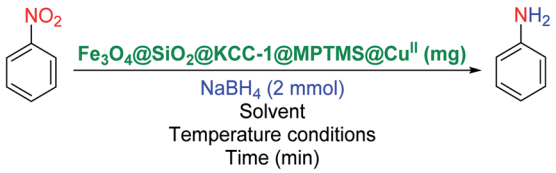


| Entry[a] | Catalyst loading (mg) | Solvent | Temperature conditions | Time (min) | Conversion (%) |
|---|---|---|---|---|---|
| 1 | 10 | $H_2O$ | 60 °C | 5 | 100 |
| 2 | 20 | $H_2O$ | 60 °C | 5 | 100 |
| 3 | 10 | $CH_3OH$ | Reflux | 120 | 20 |
| 4 | 10 | $CH_3CH_2OH$ | Reflux | 120 | 20 |
| 5 | 10 | $CH_3CN$ | Reflux | 120 | 10 |
| 6 | 10 | *n*-Hexane | Reflux | 120 | 0 |
| 7 | 10 | $CH_2Cl_2$ | Reflux | 120 | 0 |

[a] All reactions were carried out with 1 mmol of $PhNO_2$ in 3 mL of solvent.

Table 2 Reduction of nitroarenes to corresponding arylamines using $NaBH_4$ catalyzed by the $Fe_3O_4$@$SiO_2$@KCC-1@MPTMS@$Cu^{II}$ nanocomposite in water[f]

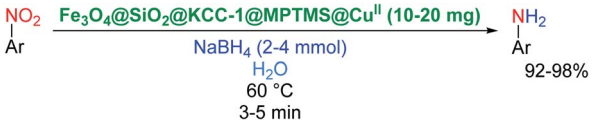


| Entry[a] | Substrate | Product | RMCR[b] | Time (min) | Yield[c] (%) | TON[d] | TOF[e] ($min^{-1}$) |
|---|---|---|---|---|---|---|---|
| 1 | 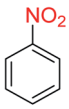 | 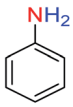 | 1 : 2 : 10 | 5 | 98 | 44.166 | 8.833 |
| 2 | 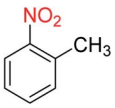 | 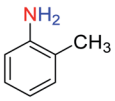 | 1 : 2 : 10 | 3 | 95 | 42.814 | 14.271 |
| 3 | 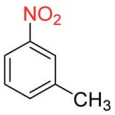 | 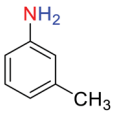 | 1 : 2 : 10 | 3 | 94 | 42.364 | 14.121 |
| 4 | 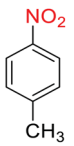 | 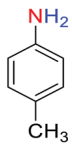 | 1 : 2 : 10 | 3 | 94 | 42.364 | 14.121 |
| 5 | 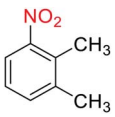 | 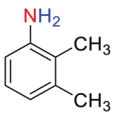 | 1 : 2 : 10 | 4 | 96 | 43.265 | 10.816 |
| 6 | 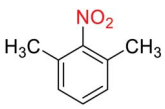 | 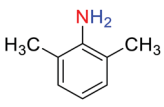 | 1 : 2 : 10 | 5 | 96 | 43.265 | 8.653 |

Table 2 (*Contd.*)

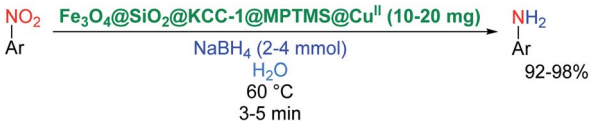


| Entry[a] | Substrate | Product | RMCR[b] | Time (min) | Yield[c] (%) | TON[d] | TOF[e] ($min^{-1}$) |
|---|---|---|---|---|---|---|---|
| 7 | 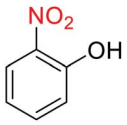 | 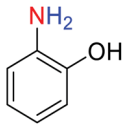 | 1 : 2 : 10 | 4 | 93 | 41.913 | 10.478 |
| 8 | 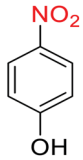 | 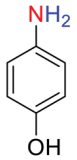 | 1 : 2 : 10 | 4 | 93 | 41.913 | 10.478 |
| 9 | 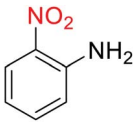 |  | 1 : 2 : 10 | 3 | 94 | 42.364 | 14.121 |
| 10 | 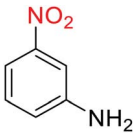 | 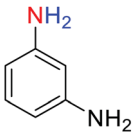 | 1 : 2 : 10 | 4 | 97 | 43.716 | 10.929 |
| 11 | 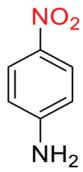 | 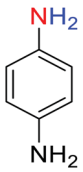 | 1 : 2 : 10 | 3 | 95 | 42.814 | 14.271 |
| 12 | 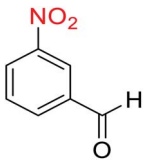 | 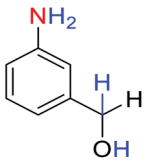 | 1 : 4 : 20 | 4 | 92 | 20.731 | 5.182 |
| 13 | 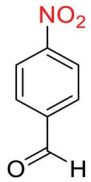 | 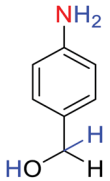 | 1 : 4 : 20 | 5 | 93 | 20.956 | 4.191 |
| 14 | 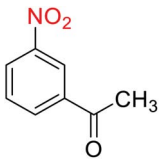 | 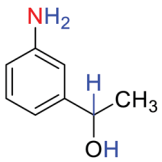 | 1 : 4 : 20 | 5 | 95 | 21.407 | 4.281 |
| 15 | 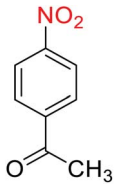 | 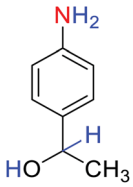 | 1 : 4 : 20 | 4 | 96 | 21.632 | 5.408 |

Table 2 (*Contd.*)

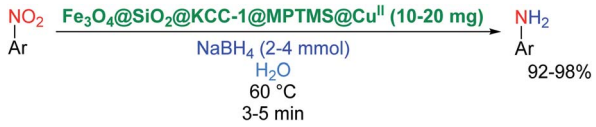


| Entry[a] | Substrate | Product | RMCR[b] | Time (min) | Yield[c] (%) | TON[d] | TOF[e] ($min^{-1}$) |
|---|---|---|---|---|---|---|---|
| 16 | 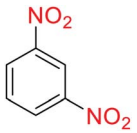 | 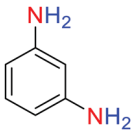 | 1 : 4 : 20 | 5 | 92 | 20.731 | 4.146 |

[a] All reactions were carried out in 3 mL of the water solvent. [b] RMCR (reaction main components ratio) = substrate (mmol) : $NaBH_4$ (mmol) : catalyst (mg). [c] Yields refer to isolated pure products. [d] TON (turnover number) = [(mol of product formed)/(mol of catalyst used)]. [e] TOF (turnover frequency) = [(mol of product formed)/(mol of catalyst used) × (time)]. [f] The TONs and TOFs values were calculated based on the existed amount of copper (Cu) in the as-prepared nanocatalyst (in 10 mg of the mesoporous nanocatalyst, 1.41 mg (or 0.022188650 mmol) of Cu has existed).

Table 3 Optimization experiments for the one-pot reductive acetylation of $PhNO_2$ using the $Fe_3O_4$@$SiO_2$@KCC-1@MPTMS@$Cu^{II}$ nanocatalyst in water

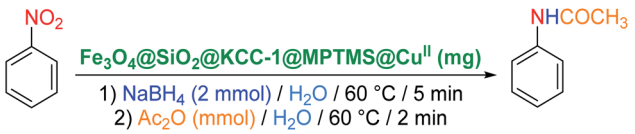


| Entry[a] | Catalyst loading (mg) | $Ac_2O$ (mmol) | Yield (%) |
|---|---|---|---|
| 1 | 10 | 1 | 95 |
| 2 | 20 | 1 | 95 |
| 3 | 10 | 2 | 95 |
| 4 | 30 | 1 | 95 |

[a] All reactions were carried out with 1 mmol of $PhNO_2$ in 3 mL of the water solvent.

performance of the mentioned nanocatalyst was more studied in the reduction of various aromatic nitro compounds under optimal reaction conditions (Table 1, entry 1). As shown in Table 2, it was found that this imperative and valuable organic transformation was carried out with acceptable results in the presence of the $Fe_3O_4$@$SiO_2$@KCC-1@MPTMS@$Cu^{II}$ mesoporous catalytic system in water. Besides, the turnover numbers (TONs) and turnover frequencies (TOFs) of the catalyst in these reduction reactions were calculated, and are listed in Table 2. Also, according to the promising results of the reduction reaction of nitroarenes, we decided to design a new and green one-pot reductive acetylation reaction for the straightforward transformation of aromatic nitro compounds to the corresponding arylacetamides. For this purpose, we performed some optimization experiments to find the best optimal conditions for this valuable organic transformation (Table 3). After these experiments and having the optimal conditions in hand (Table 3, entry 1), we expanded this one-pot reaction using a wide range of nitroarenes under green and efficient reaction conditions (Table 4). Furthermore, based on our observations and authentic scientific papers and proofs in this field, we depicted a concise and plausible mechanism for the one-pot reductive acetylation of nitroarenes in the presence of the as-prepared mesoporous $Fe_3O_4$@$SiO_2$@KCC-1@MPTMS@$Cu^{II}$ nano-based catalytic system (Scheme 2).

**2.2.2 One-pot synthesis of coumarin compounds.** The importance of the coumarins, as mentioned in the Introduction Section, drove us to introduce new, efficient, and environmentally benign approaches to the preparation of two different classes of such outstanding heterocyclic compounds. First of all, we decided to investigate the $Fe_3O_4$@$SiO_2$@KCC-1@MPTMS@$Cu^{II}$ mesoporous nanocomposite catalytic performance in the one-pot *pseudo*-three-component condensation of aromatic aldehydes (**1a–n**) and 4-hydroxycoumarin (**2**) for the preparation of bis-coumarins (**3a–n**). In this regard, we selected a model one-pot reaction between benzaldehyde (**1a**) and 4-hydroxycoumarin (**2**) in the presence of 10 mg of the mentioned as-prepared $Cu^{II}$-containing mesoporous nanocatalyst, which was carried out in different types of solvents including $H_2O$, $CH_3OH$, $CH_3CH_2OH$, $CH_3CN$, *n*-hexane, EtOAc, and $CH_2Cl_2$ under reflux conditions (Table 5, entries 1–7). In addition, we tested the solvent-free conditions upon model reaction at 70 °C, and it was found that the mentioned protocol is efficient compared with others (Table 5, entry 8). Notably, the decreasing and or even increasing amount of the mentioned nanocatalyst had no positive effect on the reaction time or yield of the desired product (Table 5, entries 9 and 10). In addition, we designed and conducted some control experiments using component parts of the $Fe_3O_4$@$SiO_2$@KCC-1@MPTMS@$Cu^{II}$ nanocomposite (Table 5, entries 11–14). To our delight, the control experiments results indicated that the catalytic effect of the as-prepared nanocomposite is definitely better than that of its components. With the optimal

Table 4 One-pot reductive acetylation of nitroarenes catalyzed by the $Fe_3O_4$@$SiO_2$@KCC-1@MPTMS@$Cu^{II}$ nanocomposite in water[f]

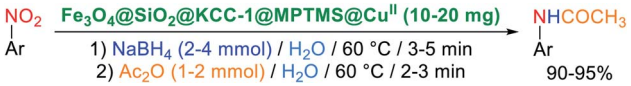


| Entry[a] | Substrate | Product | RMCR[b] | Time (min) | Yield[c] (%) | TON[d] | TOF[e] ($min^{-1}$) |
|---|---|---|---|---|---|---|---|
| 1 | 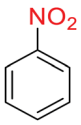 | 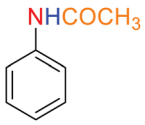 | 1 : 2 : 10 : 1 | 7 | 95 | 42.814 | 6.116 |
| 2 | 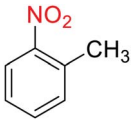 | 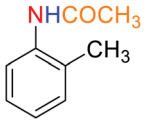 | 1 : 2 : 10 : 1 | 5 | 94 | 42.364 | 8.472 |
| 3 | 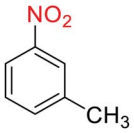 | 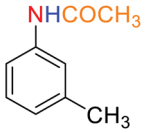 | 1 : 2 : 10 : 1 | 5 | 95 | 42.814 | 8.562 |
| 4 | 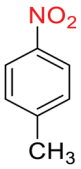 | 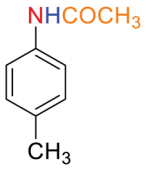 | 1 : 2 : 10 : 1 | 5 | 90 | 40.561 | 8.112 |
| 5 | 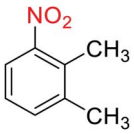 | 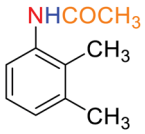 | 1 : 2 : 10 : 1 | 7 | 94 | 42.364 | 6.052 |
| 6 | 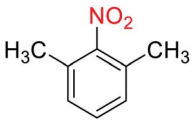 | 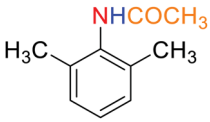 | 1 : 2 : 10 : 1 | 7 | 92 | 41.462 | 5.923 |
| 7 | 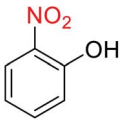 | 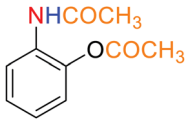 | 1 : 2 : 10 : 2 | 7 | 90 | 40.561 | 5.794 |
| 8 | 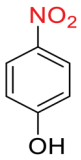 | 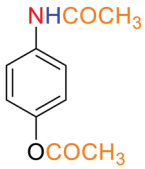 | 1 : 2 : 10 : 2 | 5 | 90 | 40.561 | 8.112 |
| 9 | 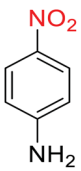 | 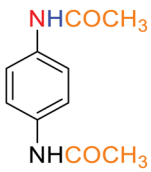 | 1 : 2 : 10 : 2 | 5 | 91 | 41.011 | 8.202 |
| 10 | 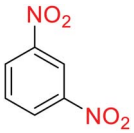 | 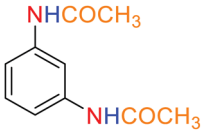 | 1 : 4 : 20 : 2 | 7 | 94 | 21.182 | 3.026 |

[a] All reactions were carried out in 3 mL of the water solvent. [b] RMCR (reaction main components ratio) = substrate (mmol) : $NaBH_4$ (mmol) : catalyst (mg) : $Ac_2O$ (mmol). [c] Yields refer to isolated pure products. [d] TON (turnover number) = [(mol of product formed)/(mol of catalyst used)]. [e] TOF (turnover frequency) = [(mol of product formed)/(mol of catalyst used) × (time)]. [f] The TONs and TOFs values were calculated based on the existed amount of copper (Cu) in the as-prepared nanocatalyst (in 10 mg of the mesoporous nanocatalyst, 1.41 mg (or 0.022188650 mmol) of Cu has existed).

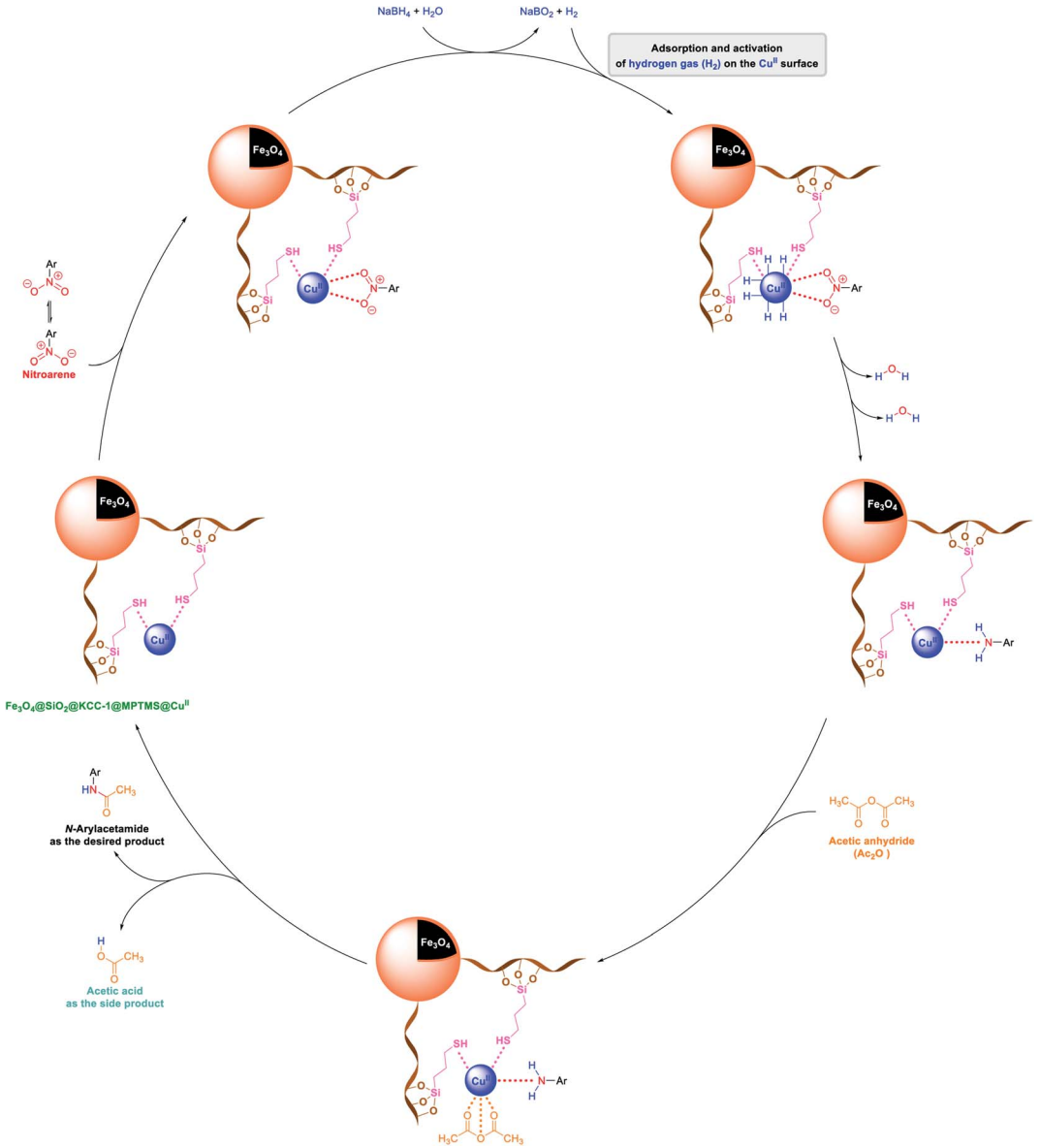


Scheme 2 Plausible mechanism of the one-pot reductive acetylation of nitroarenes catalyzed by the $Fe_3O_4$@$SiO_2$@KCC-1@MPTMS@$Cu^{II}$ nanocomposite in water.

and favorable conditions in hand (Table 5, entry 8), the scope and limitations of this $Fe_3O_4$@$SiO_2$@KCC-1@MPTMS@$Cu^{II}$ mesoporous nanocomposite-catalyzed solvent-free one-pot *pseudo*-three-component synthetic strategy were investigated using various aromatic aldehydes (**1a–n**). We were pleased to find that a wide range of bis-coumarins (**3a–n**) were successfully obtained in good-to-excellent yields along with acceptable TONs and TOFs (Scheme 3).

Also, due to the success in the one-pot synthesis of bis-coumarins (**3a–n**) using the $Fe_3O_4$@$SiO_2$@KCC-1@MPTMS@$Cu^{II}$ mesoporous catalytic system, we decided to carry out a one-pot three-component reaction between aromatic aldehydes (**1a–n**), dimedone (**4**), and malononitrile (**5**) for the synthesis of 2-amino-4-aryl-7,7-dimethyl-5-oxo-5,6,7,8-tetrahydro-4*H*-chromene-3-carbonitriles (**6a–n**) as another class of coumarin compounds in the presence of the mentioned copper$^{II}$-containing mesoporous nanocatalyst. For this purpose, we carried out some optimization experiments to find the optimal conditions (Table 6), after which (Table 6, entry 8) a series of 2-amino-4-aryl-7,7-dimethyl-5-oxo-5,6,7,8-tetrahydro-4*H*-chromene-3-carbonitriles (**6a–n**) were successfully synthesized in the presence of 30 mg of the as-prepared dendritic $Fe_3O_4$@$SiO_2$@KCC-1@MPTMS@$Cu^{II}$ nanocomposite catalytic system under solvent-free conditions at 110 °C in good-to-excellent yields and suitable TONs and TOFs (Scheme 4).

It is worthy to note that reasonable mechanisms for the solvent-free one-pot multi-component synthesis of **3a–n** and **6a–n** in the presence of the cockscomb flower-like $Fe_3O_4$@$SiO_2$@-KCC-1@MPTMS@$Cu^{II}$ mesoporous catalytic system are depicted in Schemes 5 and 6, respectively.

Table 5 Optimization reaction conditions for the *pseudo*-three-component synthesis of **3a**

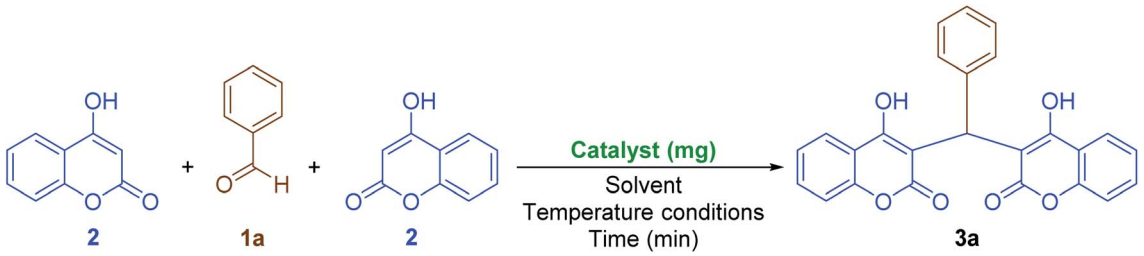


| Entry | Catalyst | Catalyst loading (mg) | Solvent | Temperature conditions | Time (min) | Yield (%) |
|---|---|---|---|---|---|---|
| 1 | $Fe_3O_4$@$SiO_2$@KCC-1@MPTMS@$Cu^{II}$ | 10 | $H_2O$ | Reflux | 60 | 70 |
| 2 | $Fe_3O_4$@$SiO_2$@KCC-1@MPTMS@$Cu^{II}$ | 10 | $CH_3OH$ | Reflux | 60 | 50 |
| 3 | $Fe_3O_4$@$SiO_2$@KCC-1@MPTMS@$Cu^{II}$ | 10 | $CH_3CH_2OH$ | Reflux | 60 | 75 |
| 4 | $Fe_3O_4$@$SiO_2$@KCC-1@MPTMS@$Cu^{II}$ | 10 | $CH_3CN$ | Reflux | 90 | 75 |
| 5 | $Fe_3O_4$@$SiO_2$@KCC-1@MPTMS@$Cu^{II}$ | 10 | *n*-Hexane | Reflux | 120 | — |
| 6 | $Fe_3O_4$@$SiO_2$@KCC-1@MPTMS@$Cu^{II}$ | 10 | EtOAc | Reflux | 120 | — |
| 7 | $Fe_3O_4$@$SiO_2$@KCC-1@MPTMS@$Cu^{II}$ | 10 | $CH_2Cl_2$ | Reflux | 120 | — |
| 8 | $Fe_3O_4$@$SiO_2$@KCC-1@MPTMS@$Cu^{II}$ | 10 | Solvent-free | 70 °C | 20 | 97 |
| 9 | $Fe_3O_4$@$SiO_2$@KCC-1@MPTMS@$Cu^{II}$ | 5 | Solvent-free | 70 °C | 20 | 80 |
| 10 | $Fe_3O_4$@$SiO_2$@KCC-1@MPTMS@$Cu^{II}$ | 15 | Solvent-free | 70 °C | 20 | 97 |
| 11 | $Fe_3O_4$@$SiO_2$@KCC-1@MPTMS | 10 | Solvent-free | 70 °C | 120 | 25 |
| 12 | $Fe_3O_4$@$SiO_2$@KCC-1 | 10 | Solvent-free | 70 °C | 120 | 10 |
| 13 | $Fe_3O_4$@$SiO_2$ | 10 | Solvent-free | 70 °C | 120 | — |
| 14 | $Fe_3O_4$ | 10 | Solvent-free | 70 °C | 120 | — |

### 2.3 A comparative study

The presented new protocols upon all the four mentioned organic transformations (namely, reduction and reductive acetylation of nitroarenes and one-pot synthesis of 3,3'-(arylmethylene)bis(4-hydroxy-2*H*-chromen-2-ones) (namely, biscoumarins) (**3a–n**) and 2-amino-4-aryl-7,7-dimethyl-5-oxo-5,6,7,8-tetrahydro-4*H*-chromene-3-carbonitriles (**6a–n**)) using the cockscomb flower-like $Fe_3O_4$@$SiO_2$@KCC-1@MPTMS@$Cu^{II}$ mesoporous nanocatalyst are advantageous over most of the previously reported methods in various terms including catalyst loading, reaction time, favorable yield, and use of green reaction medium. In Table 7, a comparison of our protocols with some previously reported protocols upon reduction and reductive acetylation of nitrobenzene ($PhNO_2$) and one-pot synthesis of **3a** and **6a** is presented.

### 2.4 Recoverability, reusability, and leaching studies of the $Fe_3O_4$@$SiO_2$@KCC-1@MPTMS@$Cu^{II}$ mesoporous catalytic system

Uncomplicated recovery process and high reusability of catalytic systems are noteworthy aspects, exclusively for commercial and industrial applications and from the green chemistry point of view. In this regard, we performed some experiments to investigate the catalyst recyclability for all the four models titled organic reactions under the optimized reaction conditions. To do this and after each investigation, the as-prepared mesoporous catalyst was separated from the reaction pot using an external magnetic field. Then, the isolated $Fe_3O_4$@$SiO_2$@KCC-1@MPTMS@$Cu^{II}$ catalyst was washed, dried, and then directly used in the next run of the reaction. As shown in Fig. 11, the recoverability and reusability experiments of the $Fe_3O_4$@$SiO_2$@KCC-1@MPTMS@$Cu^{II}$ nanocomposite revealed satisfactory results even after seven runs for all the four mentioned organic reactions. Also, to evaluate the stability of the mesoporous $Fe_3O_4$@$SiO_2$@KCC-1@MPTMS@$Cu^{II}$ nanocomposite system in the reaction environments, we carried out leaching tests based on the ICP-OES measurements, and it was found that the amount of copper (Cu) after the seventh reaction cycle was reduced approximately 4% compared with the fresh one. Furthermore, the TEM image (Fig. 12) of the recycled dendritic $Fe_3O_4$@$SiO_2$@KCC-1@MPTMS@$Cu^{II}$ catalytic system after the seventh recycling step with those of the fresh ones displays that the morphology of the mentioned nanocomposite roughly remained intact.

## 3. Experimental

### 3.1 Reagents, samples, and apparatus

All starting materials, reagents, and solvents were commercially available (purchased from Merck, Sigma-Aldrich, and Fluka companies) and used directly without further purification. A SOLTEC SONICA 2400MH S3 (300 W) instrument was used for ultrasonic irradiation. FT-IR spectra were recorded using a Thermo Nicolet Nexus 670 spectrometer, and $^1$H NMR spectra

were recorded using a Bruker Avance 300 MHz and 400 MHz spectrometer. The crystalline structures of the prepared nanocomposites were analyzed by Powder X-ray diffraction (PXRD) using a Philips PANalytical X'PertPro diffractometer (Netherlands) in 40 kV and 30 mA with a monochromatized Cu Kα radiation ($\lambda$ = 1.5418 Å). The SEM images and EDX diagram were acquired using an FESEM-TESCAN MIR A3 electronic microscope. The TEM images were acquired using a Zeiss EM10C-100 kV transmission electron microscope. The elemental analysis was carried out by inductively coupled plasma-optical emission spectrometry (Optima 7300DV ICP-OES). The magnetic properties of the prepared samples were measured using a vibrating sample magnetometer (Meghnatis Daghigh, Iran) under magnetic fields up to 20 kOe. The

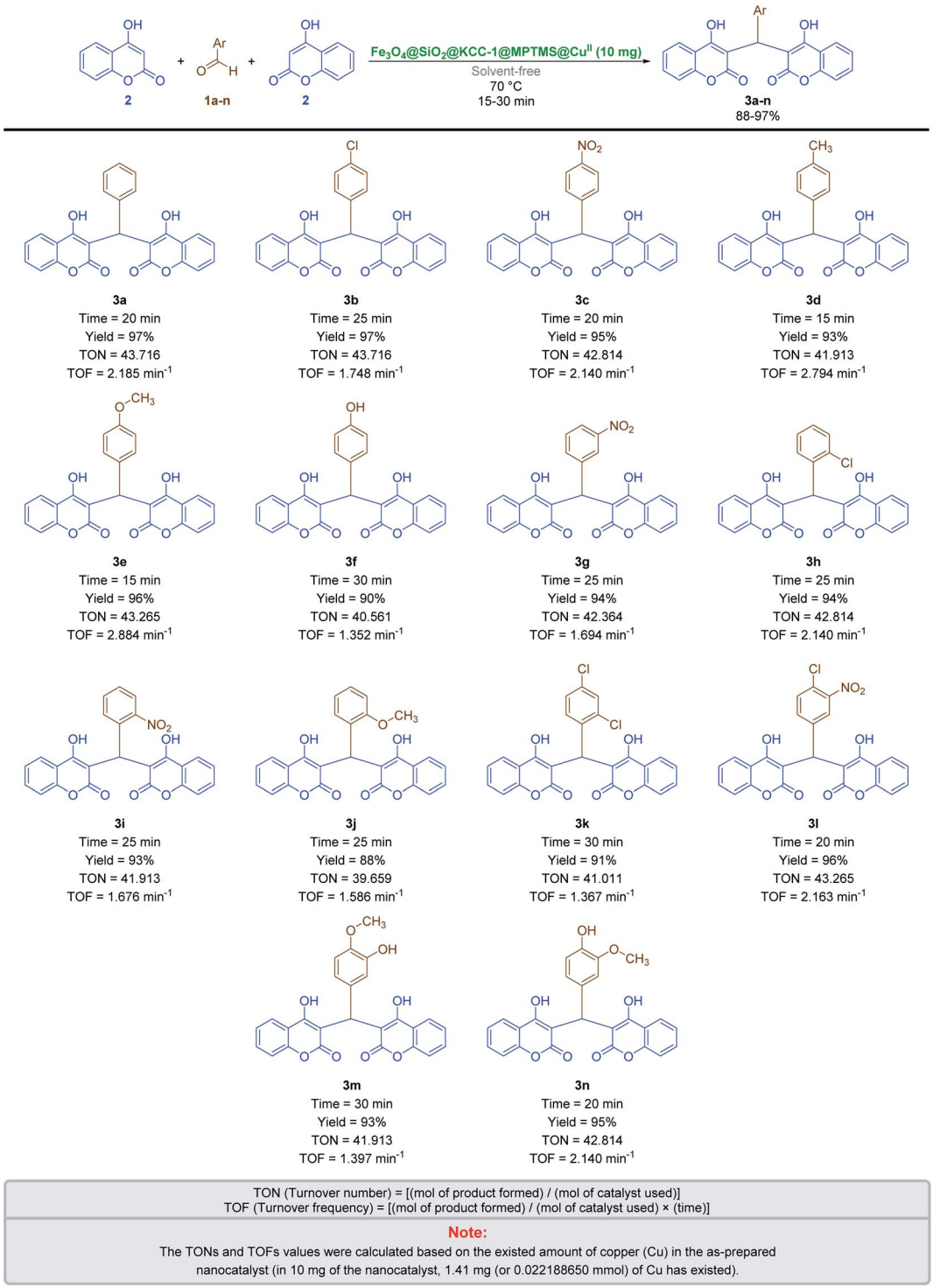


Scheme 3 Solvent-free one-pot *pseudo*-three-component synthesis of bis-coumarins (**3a–n**) catalyzed by the $Fe_3O_4$@$SiO_2$@KCC-1@MPTMS@$Cu^{II}$ nanocomposite.

Table 6 Optimization reaction conditions for the one-pot synthesis of 6a

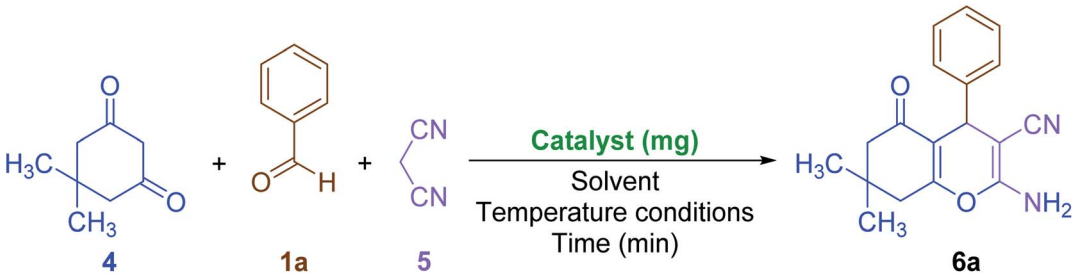


| Entry | Catalyst | Catalyst loading (mg) | Solvent | Temperature conditions | Time (min) | Yield (%) |
|---|---|---|---|---|---|---|
| 1 | $Fe_3O_4$@$SiO_2$@KCC-1@MPTMS@$Cu^{II}$ | 30 | $H_2O$ | Reflux | 120 | 60 |
| 2 | $Fe_3O_4$@$SiO_2$@KCC-1@MPTMS@$Cu^{II}$ | 30 | $CH_3OH$ | Reflux | 60 | 50 |
| 3 | $Fe_3O_4$@$SiO_2$@KCC-1@MPTMS@$Cu^{II}$ | 30 | $CH_3CH_2OH$ | Reflux | 60 | 68 |
| 4 | $Fe_3O_4$@$SiO_2$@KCC-1@MPTMS@$Cu^{II}$ | 30 | $CH_3CN$ | Reflux | 90 | 70 |
| 5 | $Fe_3O_4$@$SiO_2$@KCC-1@MPTMS@$Cu^{II}$ | 30 | *n*-Hexane | Reflux | 120 | — |
| 6 | $Fe_3O_4$@$SiO_2$@KCC-1@MPTMS@$Cu^{II}$ | 30 | EtOAc | Reflux | 120 | — |
| 7 | $Fe_3O_4$@$SiO_2$@KCC-1@MPTMS@$Cu^{II}$ | 30 | THF | Reflux | 90 | 55 |
| 8 | $Fe_3O_4$@$SiO_2$@KCC-1@MPTMS@$Cu^{II}$ | 30 | Solvent-free | 110 °C | 60 | 96 |
| 9 | $Fe_3O_4$@$SiO_2$@KCC-1@MPTMS@$Cu^{II}$ | 25 | Solvent-free | 110 °C | 60 | 84 |
| 10 | $Fe_3O_4$@$SiO_2$@KCC-1@MPTMS@$Cu^{II}$ | 35 | Solvent-free | 110 °C | 60 | 96 |
| 11 | $Fe_3O_4$@$SiO_2$@KCC-1@MPTMS | 30 | Solvent-free | 110 °C | 120 | 15 |
| 12 | $Fe_3O_4$@$SiO_2$@KCC-1 | 30 | Solvent-free | 110 °C | 120 | 10 |
| 13 | $Fe_3O_4$@$SiO_2$ | 30 | Solvent-free | 110 °C | 120 | — |
| 14 | $Fe_3O_4$ | 30 | Solvent-free | 110 °C | 120 | — |

nitrogen adsorption–desorption experiment was carried out using a Belsorp-Max, Japan. Thin-layer chromatography (TLC) was applied for the purity determination of the products and reaction monitoring over a silica gel 60 $F_{254}$ aluminum sheet.

### 3.2 Preparation of the $Fe_3O_4$ MNPs

The $Fe_3O_4$ magnetic nanoparticles (MNPs) were prepared by a chemical co-precipitation method. Typically, in a two-neck round-bottom flask, a solution of $FeCl_3 \cdot 6H_2O$ (5.838 g, 21.6 mmol) and $FeCl_2 \cdot 4H_2O$ (2.147 g, 10.8 mmol) in distilled water (100 mL) was prepared. The solution was stirred vigorously at 85 °C in a nitrogen atmosphere for ten minutes. Then, an aqueous ammonia solution (25%, 10 mL) was quickly added to the resulting solution of the iron salts at 85 °C. Upon the addition, The black $Fe_3O_4$ NPs were immediately precipitated. The prepared mixture was continuously stirred at 85 °C for thirty minutes under the nitrogen atmosphere. After cooling to room temperature, the obtained black nanoparticles were separated from the reaction pot using an external magnetic field and washed with distilled water, a solution of sodium chloride (0.02 M), and again distilled water. Drying under an air atmosphere affords the pure $Fe_3O_4$ MNPs.

### 3.3 Preparation of the $Fe_3O_4$@$SiO_2$ MNPs

First, the $Fe_3O_4$ MNPs (1.5 g) were dispersed in distilled water (20 mL) by sonication for twenty minutes. Then, isopropanol (200 mL) was added, and the resulting suspension was sonicated for thirty minutes. Consequently, PEG-400 (5.36 g), distilled water (20 mL), $NH_4OH$ (25%, 10 mL), and tetraethyl orthosilicate (TEOS) (2 mL) were respectively added, and the prepared mixture was stirred at room temperature for twenty-eight hours. The obtained $Fe_3O_4$@$SiO_2$ MNPs were magnetically separated, washed with distilled water and ethanol, and subsequently dried under an air atmosphere.

### 3.4 Preparation of the $Fe_3O_4$@$SiO_2$@KCC-1 magnetic nanocomposite

A suspension of the $Fe_3O_4$@$SiO_2$ MNPs (0.25 g) in an aqueous solution of urea (0.3 g urea in 30 mL distilled water) was prepared. Then, the mentioned mixture was sonicated for one hour. In another vessel, a solution of cetyltrimethylammonium bromide (CTAB) (0.5 g) in a mixture of *n*-pentanol (0.75 mL) and cyclohexane (30 mL) was prepared. Next, the suspensions of the $Fe_3O_4$@$SiO_2$ MNPs and CTAB were mixed together, and the resulting mixture was stirred at room temperature for five minutes. After that, TEOS (1.25 g) was added in a drop-wise manner, and the mixture was continuously stirred at room temperature for one hour, followed by the transfer of the mixture into an autoclave (120 °C) where it is kept for five hours. In this stage, the dendritic silica was grown on the surface of the $Fe_3O_4$@$SiO_2$ MNPs, affording a fibrous $Fe_3O_4$@$SiO_2$@KCC-1 composite system, which was

magnetically separated from the reaction environment and washed with distilled water and then acetone. After that, the mentioned nanocomposite was dried in an oven at 40 °C and then calcined at 550 °C for five hours.

### 3.5 Preparation of the $Fe_3O_4$@$SiO_2$@KCC-1@MPTMS magnetic nanocomposite

First, the prepared $Fe_3O_4$@$SiO_2$@KCC-1 nanocomposite (0.5 g) was dispersed by sonication for twenty minutes in toluene (20 mL). Then, (3-mercaptopropyl)trimethoxysilane (MPTMS) (0.7 mL) was added into the mentioned suspension in a dropwise manner. The resulting mixture was then stirred under reflux conditions for twenty hours under the nitrogen atmosphere. After that, the mixture was cooled to room temperature, and the prepared $Fe_3O_4$@$SiO_2$@KCC-1@MPTMS nanocomposite was magnetically separated from the reaction pot, washed with ethanol, and then dried in an oven at 80 °C.

### 3.6 Preparation of the $Fe_3O_4$@$SiO_2$@KCC-1@MPTMS@$Cu^{II}$ magnetic nanocomposite

In a round-bottom flask, the prepared $Fe_3O_4$@$SiO_2$@KCC-1@MPTMS (0.6 g) was dispersed in water (50 mL) by ultrasound irradiation for twenty minutes. Then, copper$^{II}$ nitrate hexahydrate ($Cu(NO_3)_2 \cdot 6H_2O$) (0.59 g, 2 mmol) and sodium carbonate ($Na_2CO_3$) (0.424 g, 4 mmol) were added into the mentioned reaction pot and sonicated for another twenty minutes. The resulting mixture was stirred under reflux conditions for twenty hours. The obtained cockscomb flower-like $Fe_3O_4$@$SiO_2$@KCC-1@MPTMS@$Cu^{II}$ mesoporous nanocomposite system was magnetically separated from the reaction pot, washed with ethanol, and then dried in an oven at 50 °C.

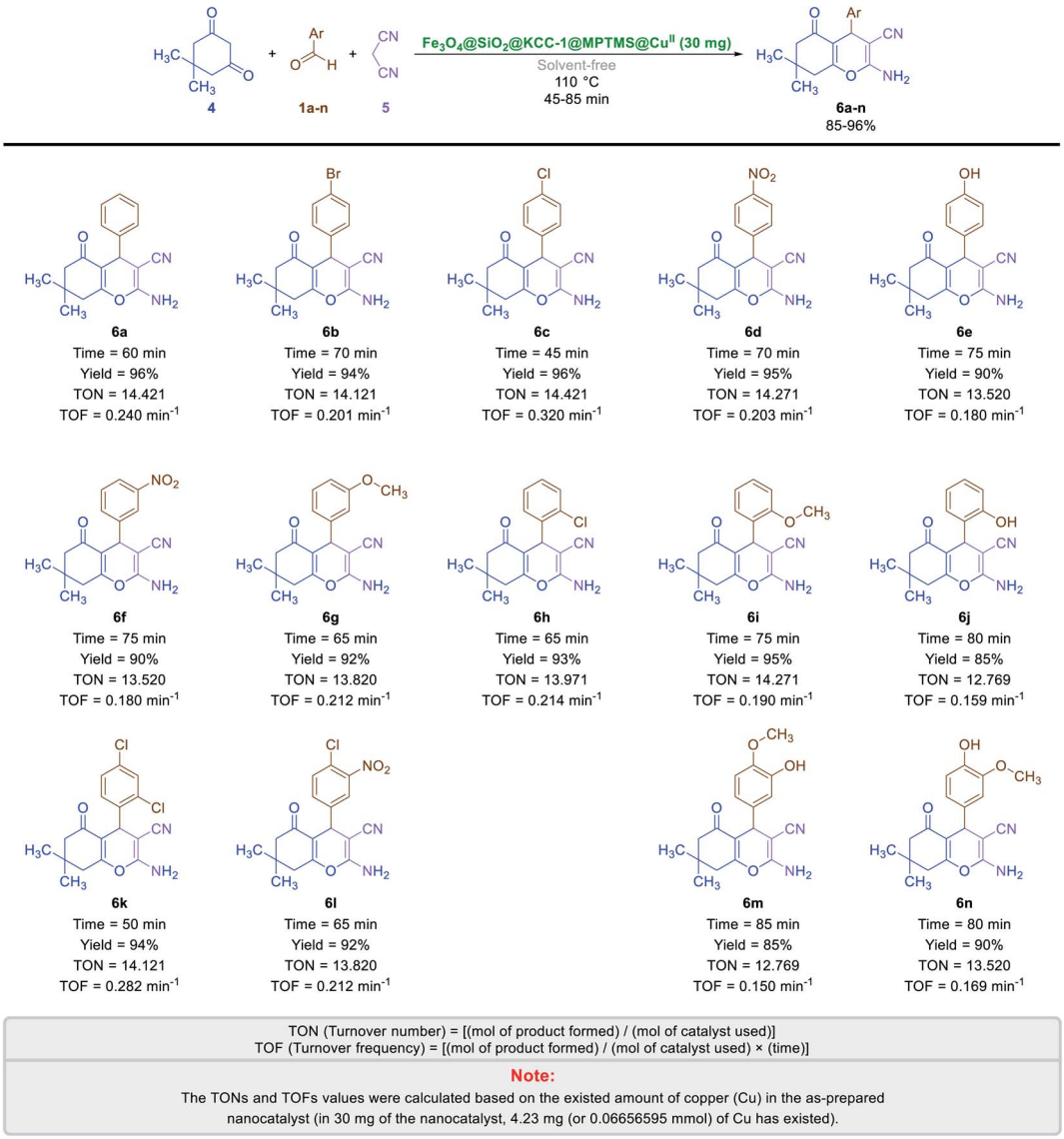


Scheme 4 Solvent-free one-pot three-component synthesis of 2-amino-4-aryl-7,7-dimethyl-5-oxo-5,6,7,8-tetrahydro-4*H*-chromene-3-carbonitriles (**6a–n**) catalyzed by the $Fe_3O_4$@$SiO_2$@KCC-1@MPTMS@$Cu^{II}$ nanocomposite.

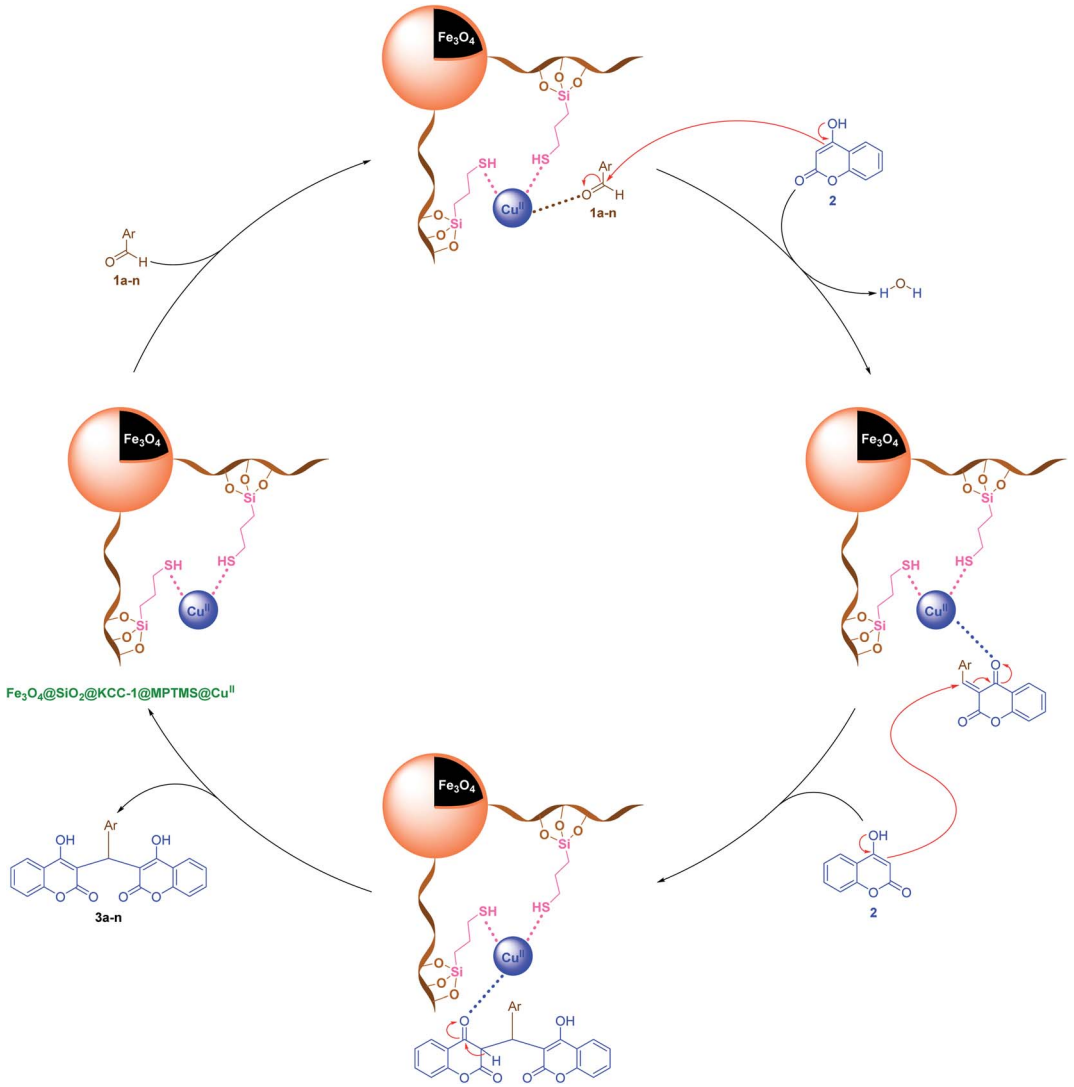


Scheme 5 Plausible mechanism for the solvent-free one-pot *pseudo*-three-component synthesis of bis-coumarins (**3a–n**) catalyzed by the $Fe_3O_4$@$SiO_2$@KCC-1@MPTMS@$Cu^{II}$ nanocomposite.

### 3.7 General procedure for the reduction of nitroarenes to arylamines catalyzed by the $Fe_3O_4$@$SiO_2$@KCC-1@MPTMS@$Cu^{II}$ nanocomposite

For example, in a round-bottom flask (15 mL) equipped with a magnetic stirrer, a mixture of $PhNO_2$ (0.123 g, 1 mmol) and $H_2O$ (3 mL) was prepared. Then, 10 mg of the as-prepared $Fe_3O_4$@$SiO_2$@KCC-1@MPTMS@$Cu^{II}$ mesoporous nanocomposite was added, and the mixture was stirred. At the next step, $NaBH_4$ (0.076 g, 2 mmol) was added, and the resulting mixture was continuously stirred at 60 °C for five minutes. After the completion of the reaction, the mixture was cooled to room temperature, and the mentioned $Cu^{II}$-containing catalytic system was separated from the reaction pot using an external magnet. The reaction mixture was extracted with dichloromethane (DCM) (3 × 5 mL) and then dried over anhydrous sodium sulfate ($Na_2SO_4$). Finally, the solvent was evaporated under reduced pressure to afford the the pure liquid aniline in 98% yield.

### 3.8 General procedure for the one-pot reductive acetylation of nitroarenes catalyzed by the $Fe_3O_4$@$SiO_2$@KCC-1@MPTMS@$Cu^{II}$ nanocomposite

As an example, $PhNO_2$ (0.123 g, 1 mmol) was mixed with 3 mL of $H_2O$ in a 15 mL round-bottom flask equipped with a magnetic stirrer. Then, the $Fe_3O_4$@$SiO_2$@KCC-1@MPTMS@$Cu^{II}$ mesoporous nanocatalyst (10 mg) was added, and the mixture was stirred. Following this, $NaBH_4$ (0.076 g, 2 mmol) was added, and the resulting mixture was stirred at 60 °C for five minutes. After the completion of the reduction reaction, acetic anhydride ($Ac_2O$) (0.102 g, 1 mmol) was added to the reaction mixture, followed by stirring for further two minutes at the same temperature. Afterward, the mixture was cooled to room temperature, and the $Fe_3O_4$@$SiO_2$@KCC-1@MPTMS@$Cu^{II}$ mesoporous nanocatalyst was separated using an external magnet. Then, the reaction mixture was extracted with DCM (3 × 5 mL) and then dried over

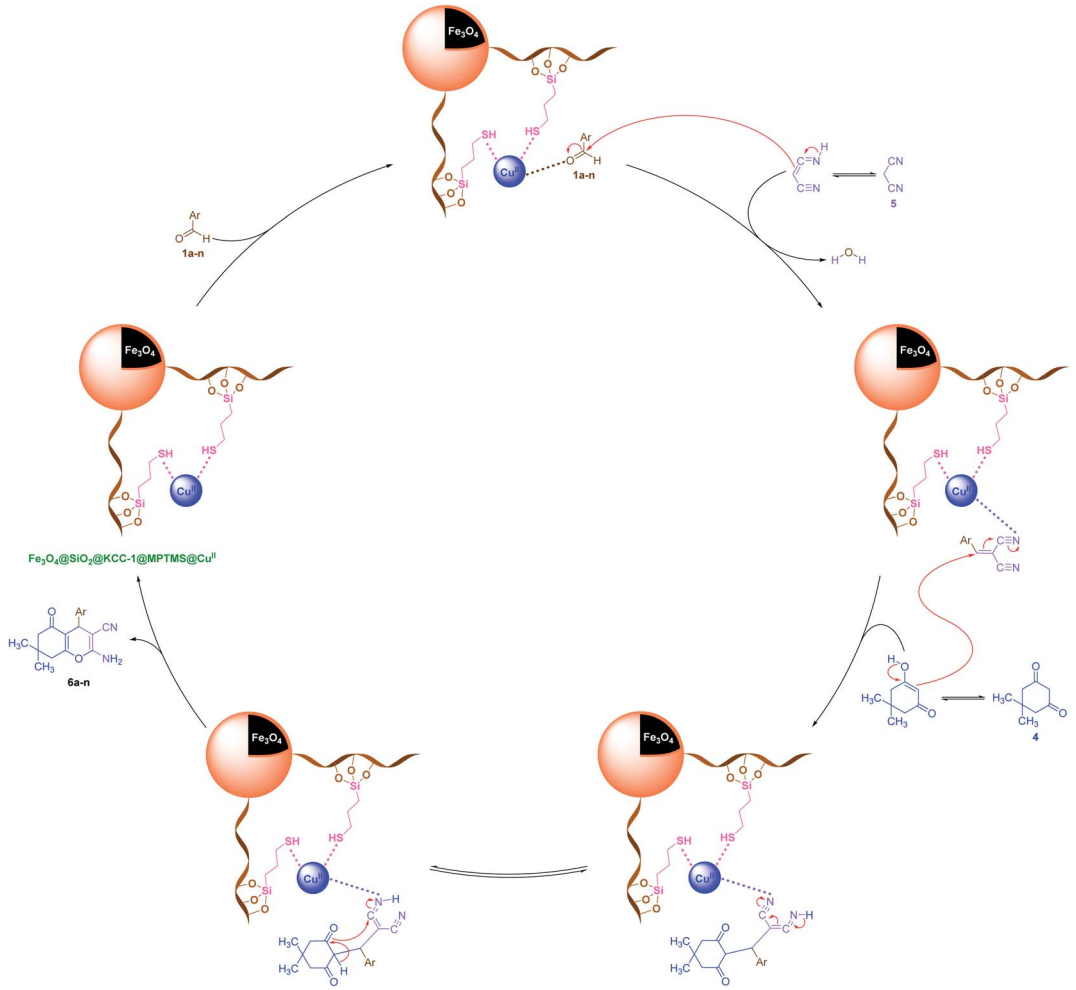


Scheme 6 Plausible mechanism for the solvent-free one-pot three-component synthesis of 2-amino-4-aryl-7,7-dimethyl-5-oxo-5,6,7,8-tetrahydro-4*H*-chromene-3-carbonitriles (**6a–n**) catalyzed by the $Fe_3O_4$@$SiO_2$@KCC-1@MPTMS@$Cu^{II}$ nanocomposite.

$Na_2SO_4$. Finally, evaporation of the solvent under reduced pressure afforded the pure acetanilide in 95% yield.

### 3.9 General procedure for the solvent-free one-pot *pseudo*-three-component synthesis of bis-coumarins (3a–n) catalyzed by the $Fe_3O_4$@$SiO_2$@KCC-1@MPTMS@$Cu^{II}$ nanocomposite

As a representative example, in a simple experimental tube, equipped with a magnetic stirrer, a mixture of benzaldehyde (0.106 g, 1 mmol), 4-hydroxycoumarin (0.324 g, 2 mmol), and the as-prepared $Fe_3O_4$@$SiO_2$@KCC-1@MPTMS@$Cu^{II}$ mesoporous nanocatalyst (10 mg) was prepared and heated at 70 °C under solvent-free conditions for twenty minutes. After completion, the mentioned one-pot *pseudo*-three-component reaction, the $Fe_3O_4$@$SiO_2$@KCC-1@MPTMS@$Cu^{II}$ nanocatalyst, was separated from the reaction pot using an external magnet. After cooling to room temperature, the resulting mixture was extracted with ethanol (2 × 5 mL), followed by drying over $Na_2SO_4$. The solvent evaporation under reduced pressure afforded the crude 3,3'-(phenylmethylene)bis(4-hydroxy-2*H*-chromen-2-one) (**3a**), which was purified by recrystallization with hot ethanol.

### 3.10 General procedure for the solvent-free one-pot three-component synthesis of 2-amino-4-aryl-7,7-dimethyl-5-oxo-5,6,7,8-tetrahydro-4*H*-chromene-3-carbonitriles (6a–n) catalyzed by the $Fe_3O_4$@$SiO_2$@KCC-1@MPTMS@$Cu^{II}$ nanocomposite

As a representative example, in a simple experimental tube, equipped with a magnetic stirrer, a mixture of benzaldehyde (0.106 g, 1 mmol), malononitrile (0.066 g, 1 mmol), 5,5-dimethyl-1,3-cyclohexanedione (0.140 g, 1 mmol), and the as-prepared $Fe_3O_4$@$SiO_2$@KCC-1@MPTMS@$Cu^{II}$ mesoporous nanocatalyst (30 mg) was prepared and heated at 110 °C under solvent-free conditions for sixty minutes. After completion of the mentioned one-pot three-component reaction and cooling down to room temperature, ethanol (3 mL) was added, and the reaction mixture was stirred for two minutes. Then, the $Fe_3O_4$@$SiO_2$@KCC-1@MPTMS@$Cu^{II}$ nanocatalyst was magnetically separated from the reaction environment. Drying over $Na_2SO_4$ and then evaporation of the solvent under reduced pressure afforded the pure 2-amino-4-phenyl-7,7-dimethyl-5-oxo-5,6,7,8-tetrahydro-4*H*-chromene-3-carbonitriles (**6a**).

Table 7 Comparison of the catalytic activity of the as-prepared $Fe_3O_4$@$SiO_2$@KCC-1@MPTMS@$Cu^{II}$ mesoporous nanocomposite with that of the samples reported in the literature upon reduction and reductive acetylation of nitrobenzene ($PhNO_2$) and one-pot synthesis of **3a**, and **6a**

Part A


| Entry | Reaction conditions | Time | Yield | Ref. |
|---|---|---|---|---|
| A1 | $Fe_3O_4$@$SiO_2$@KCC-1@MPTMS@$Cu^{II}$ (10 mg); $NaBH_4$ (2 mmol); $H_2O$; 60 °C | 5 min | 98% | *a* |
| A2 | $Ni_2B$@$Cu_2O$ (54 mg); $NaBH_4$ (2.5 mmol); wet-solvent-free grinding; room temperature | 1 min | 98% | 52*a* |
| A3 | $Ni_2B$@$CuCl_2$ (52 mg); $NaBH_4$ (2.5 mmol); wet-solvent-free grinding; room temperature | 2 min | 98% | 52*a* |
| A4 | $CuFe_2O_4$ (48 mg); $NaBH_4$ (2 mmol); $H_2O$; reflux | 50 min | 95% | 52*c* |
| A5 | (7 wt%) Pd/C (30 mg); $NaBH_4$ (2 mmol); $H_2O$; reflux | 7 min | 93% | 52*i* |
| A6 | $FeS_x$-$Fe_2O_3$@CN-*8* (10 mg); $NH_2NH_2 \cdot H_2O$ (3.2 mmol); $CH_3CH_2OH$; 85 °C | 2 h | 99.1% | 53 |
| A7 | $Ru_xPd_y$@rGO (10 mg); $NH_3BH_3$ (3 mmol); $CH_3OH$ : $H_2O$ (7 : 3); room temperature | 10 min | >99% | 54 |
| A8 | $Fe_2Se_2CO_9$ (3 mol%); $NH_2NH_2 \cdot H_2O$ (2 mmol); $H_2O$; 110 °C | 15 min | 89% | 55 |
| A9 | CuO (5 mol%); $H_3NBH_3$ (3 mmol); $CH_3OH$; 50 °C | 20 min | 93% | 56 |
| A10 | Clin@Py-Tzl@Pd (56 mg); $NaBH_4$ (2 mmol); $H_2O$ : THF (10 : 1); room temperature | 1 h | 99% | 57 |
| A11 | $Ni(OH)_2$@PANI-1 (3.2 mol%); $NaBH_4$ (10 mmol); $H_2O$; reflux | 1.5 h | 85% | 58 |
| A12 | $Fe_3O_4$/Pectin/Au (10 mg); $NH_2NH_2 \cdot H_2O$ (3 mmol); $H_2O$ : $CH_3CH_2OH$ (2 : 1); 90 °C | 1 h | 98% | 59 |
| A13 | $Mn^{II}$–Pd@L-dopa-ZnO/$Fe_3O_4$ (100 mg); $H_2$ atmosphere; $CH_3CH_2OH$ : $H_2O$ (2 : 1); room temperature | 28 min | 88% | 60 |
| A14 | Cu-BTC@$Fe_3O_4$ (15 mg); $NaBH_4$ (4 mmol); $CH_3CH_2OH$ : $H_2O$ (3 : 1); 45 °C | 3 h | 99% | 61 |
| A15 | Pd@SBA-15/TET (5 mg); $NaBH_4$ (5 mmol); $H_2O$; room temperature | 9 min | 99% | 62 |
| A16 | IT-MHAP-Ag (60 mg); $NaBH_4$ (5 mmol); $H_2O$; reflux | 25 min | 98% | 63 |
| A17 | MMT@$Fe_3O_4$@Cu (20 mg); $NaBH_4$ (3 mmol); $H_2O$; 60 °C | 5 min | 96% | 64 |
| A18 | $Fe_3O_4$@$SiO_2$@Cu–Ni–Fe–Cr LDH (10 mg); $NaBH_4$ (3 mmol); $H_2O$; 60–70 °C | 8 min | 95% | 65 |
| A19 | PSeCN/Ag (20 mg); $NaBH_4$ (5 mmol); $H_2O$; 75 °C | 25 min | 99% | 66 |

Part B


| Entry | Reaction conditions | Time | Yield | Ref. |
|---|---|---|---|---|
| B1 | $Fe_3O_4$@$SiO_2$@KCC-1@MPTMS@$Cu^{II}$ (10 mg); $NaBH_4$ (2 mmol); $Ac_2O$ (1 mmol); $H_2O$; 60 °C | 7 min | 95% | *a* |
| B2 | $Ni_2B$@$Cu_2O$ (54 mg); $NaBH_4$ (2.5 mmol); $Ac_2O$ (1 mmol); wet-solvent-free grinding; 40 °C | 2 min | 97% | 52*b* |
| B3 | $Ni_2B$@$CuCl_2$ (52 mg); $NaBH_4$ (2.5 mmol); $Ac_2O$ (1 mmol); wet-solvent-free grinding; 40 °C | 3 min | 97% | 52*b* |
| B4 | $Cu(Hdmg)_2$ (10 mol%); $NaBH_4$ (3 mmol); EtOAc (3 mL); 60 °C | 170 min | 97% | 52*d* |
| B5 | $CuFe_2O_4$ (48 mg); $NaBH_4$ (2 mmol); $Ac_2O$ (1 mmol); $H_2O$; reflux | 11 min | 97% | 52*e* |
| B6 | (7 wt%) Pd/C (30 mg); $NaBH_4$ (2 mmol); $Ac_2O$ (1 mmol); $H_2O$; reflux | 8 min | 88% | 52*i* |
| B7 | MMT@$Fe_3O_4$@Cu (20 mg); $NaBH_4$ (3 mmol); $Ac_2O$ (1 mmol); $H_2O$; 60 °C | 7 min | 97% | 64 |
| B8 | $Fe_3O_4$@$SiO_2$@Cu–Ni–Fe–Cr LDH (10 mg); $NaBH_4$ (3 mmol); $Ac_2O$ (1 mmol); $H_2O$; 60–70 °C | 8 min | 95% | 65 |
| B9 | $Fe_3O_4$@$Cu(OH)_x$ (60 mol%); $NaBH_4$ (3 mmol); $Ac_2O$ (1 mmol); $H_2O$; 60–70 °C | 6 min | 94% | 67 |
| B10 | (2 wt%) Pd/(5 wt%) Sn–$Al_2O_3$ (50 mg); $H_2$ atmosphere; $Ac_2O$ (1 mmol); $H_2O$; room temperature | 3 h | 98% | 68 |
| B11 | $NiFe_2O_4$@Cu (150 mg); $NaBH_4$ (2.5 mmol); $Ac_2O$ (2 mmol); $H_2O$ : $CH_3CH_2OH$ (3 : 1); 70 °C | 2 min | 95% | 69 |

Part C

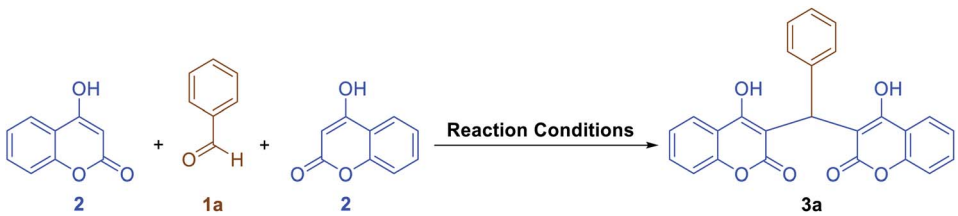


| Entry | Reaction conditions | Time | Yield | Ref. |
|---|---|---|---|---|
| C1 | $Fe_3O_4$@$SiO_2$@KCC-1@MPTMS@$Cu^{II}$ (10 mg); solvent-free; 70 °C | 20 min | 97% | *a* |
| C2 | HAP/$Fe_3O_4$ (5 mg); solvent-free; 90 °C | 60 min | 95% | 70 |
| C3 | BFA (10 wt%); $H_2O$; room temperature | 15 min | 92% | 71 |
| C4 | $Ni^0$-mont (20 mg); solvent-free; microwave irradiation (850 W) | 5 min | 95% | 72 |

Table 7 (*Contd.*)

Part C

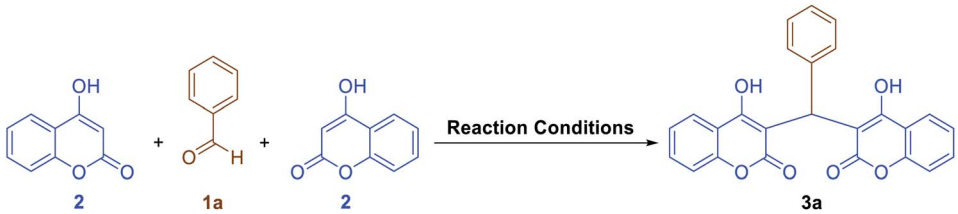


| Entry | Reaction conditions | Time | Yield | Ref. |
|---|---|---|---|---|
| C5 | Carbon-$SO_3H$ (30 mg); $H_2O$ : $CH_3CH_2OH$ (1 : 1); 80 °C | 10 min | 97% | 73 |
| C6 | $P_4VPy$-CuO (20 mg); $H_2O$; reflux | 20 min | 90% | 74 |
| C7 | RHA-$SO_3H$ (40 mg); $H_2O$; 80 °C | 15 min | 90% | 75 |
| C8 | $SO_3H@Fe_3O_4$ (15 mg); solvent-free; 80 °C | 10 min | 92% | 76 |
| C9 | $Fe(SD)_3$ (20 mol%); $H_2O$; 100 °C | 10 min | 79% | 77 |
| C10 | $Fe_3O_4@SiO_2$@Im-bisethylFc [$HC_2O_4$] (4 mg); $CH_3CH_2OH$; reflux | 1 h | 96% | 78 |
| C11 | Vitamin $B_1$ (1 mol%); solvent-free; room temperature | 1 h | 96% | 79 |
| C12 | $(N_2H_5)_2SiF_6$ (0.2 mol%); $CH_3CH_2OH$; reflux | 3 min | 95% | 80 |

Part D

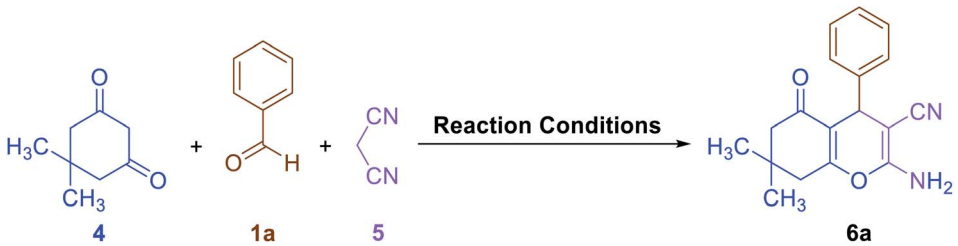


| Entry | Reaction conditions | Time | Yield | Ref. |
|---|---|---|---|---|
| D1 | $Fe_3O_4@SiO_2$@KCC-1@MPTMS@$Cu^{II}$ (30 mg); solvent-free; 110 °C | 60 min | 96% | [a] |
| D2 | $Fe_3O_4$@MCM-41@Zr (30 mg); $H_2O$ : $CH_3CH_2OH$ (3 : 7); 75 °C | 40 min | 74% | 81 |
| D3 | $Zn_2SnO_4$–$SnO_2$ (25 mg); $CH_3CH_2OH$; ultrasonic irradiation (80 °C) | 120 min | 80% | 82 |
| D4 | AMBA-$Fe_3O_4$ (50 mg); $CH_3CH_2OH$; 60 °C | 21 min | 92% | 83 |
| D5 | HMS/Pr-Rh-Zr (50 mg); PEG; 80 °C | 30 min | 87% | 84 |
| D6 | $BaFe_{12}O_{19}$@IM (12 mg); $CH_3CH_2OH$; reflux | 20 min | 88% | 85 |
| D7 | MNPs-$PhSO_3H$ (10 mg); $H_2O$ : $CH_3CH_2OH$ (1 : 1); 100 °C | 10 min | 91% | 86 |
| D8 | Bis-Su (10 mg); $H_2O$ : $CH_3CH_2OH$ (1 : 1); 80 °C | 35 min | 84% | 87 |
| D9 | Ni@Fe-doped $CeO_2$/Chitosan (10 wt%); $CH_3CH_2OH$; 60 °C | 10 min | 90% | 88 |
| D10 | $Fe_3O_4@SiO_2$-guanidine-PAA (50 mg); $H_2O$; 70 °C | 35 min | 96% | 89 |
| D11 | $Fe_3O_4$@GOQD-*O*-(propane-1-sulfonic acid) (50 mg); $H_2O$; room temperature | 35 min | 93% | 90 |

[a] Present work.

## 4. Conclusion

In conclusion, our research group has successfully prepared $Fe_3O_4@SiO_2$@KCC-1@MPTMS@$Cu^{II}$ as a new cockscomb flower-like mesoporous nanocomposite, which was fully characterized by various techniques including FT-IR, PXRD, SEM, TEM, SEM-based EDX, ICP-OES, TGA/DTA, VSM, UV-Vis, and BET and BJH analyses. Then, the as-prepared $Fe_3O_4@SiO_2$@-KCC-1@MPTMS@$Cu^{II}$ mesoporous nanocomposite was applied as an efficient catalytic system in the reduction and reductive acetylation of nitroarenes in a water medium and solvent-free one-pot synthesis of some coumarin compounds. The TONs and TOFs of the mentioned catalyst were calculated upon all the titled reactions. Notably, the mentioned as-prepared mesoporous nanocatalyst was recovered from the reaction pots using a simple magnet and reused for at least seven cycles without significant loss in activity, which ensures its good stability. In addition, in comparison with the previously reported methods (for all of the mentioned organic reactions), the presented new strategies are a viable alternative to most of them in many respects.

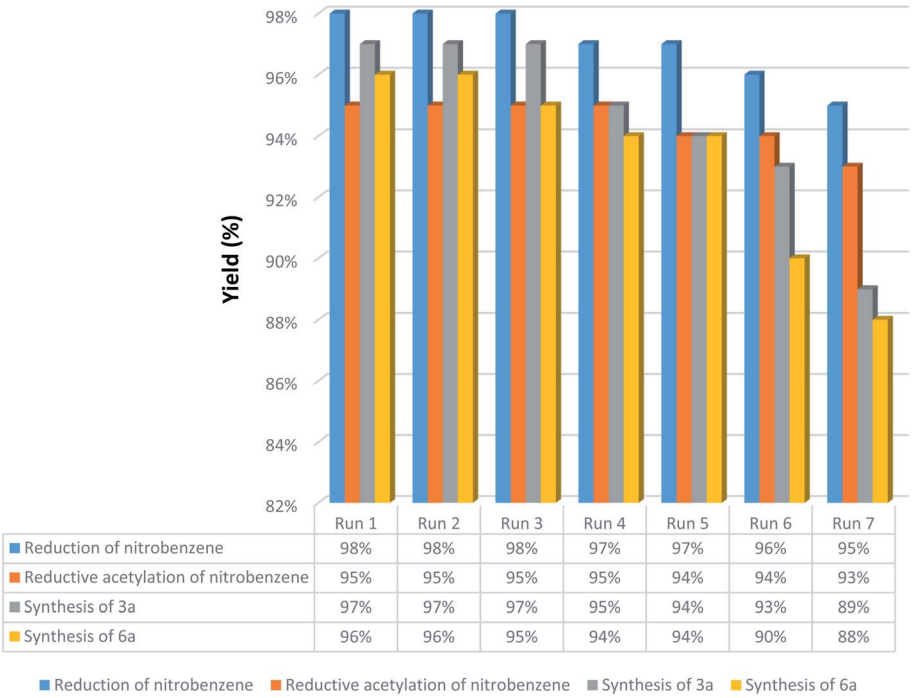


| | Run 1 | Run 2 | Run 3 | Run 4 | Run 5 | Run 6 | Run 7 |
|---|---|---|---|---|---|---|---|
| Reduction of nitrobenzene | 98% | 98% | 98% | 97% | 97% | 96% | 95% |
| Reductive acetylation of nitrobenzene | 95% | 95% | 95% | 95% | 94% | 94% | 93% |
| Synthesis of 3a | 97% | 97% | 97% | 95% | 94% | 93% | 89% |
| Synthesis of 6a | 96% | 96% | 95% | 94% | 94% | 90% | 88% |

Fig. 11 Recoverability and reusability experiments of the dendritic $Fe_3O_4$@$SiO_2$@KCC-1@MPTMS@$Cu^{II}$ mesoporous nanocomposite.

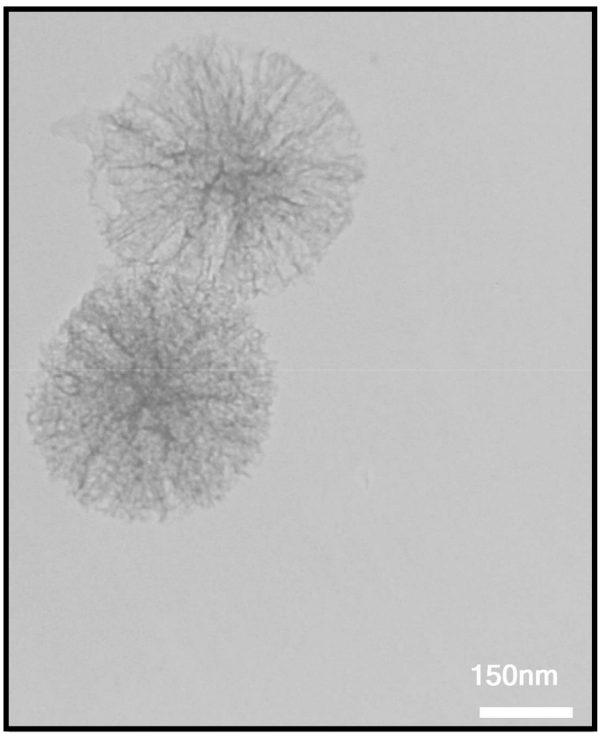


Fig. 12 TEM image of the recycled $Fe_3O_4$@$SiO_2$@KCC-1@MPTMS@$Cu^{II}$ mesoporous nanocomposite.

## Conflicts of interest

There are no conflicts to declare.

## Acknowledgements

The authors thank Urmia University for support of this work.

## References

1 (*a*) H. C. Erythropel, J. B. Zimmerman, T. M. de Winter, L. Petitjean, F. Melnikov, C. H. Lam, A. W. Lounsbury, K. E. Mellor, N. Z. Janković, Q. Tu, L. N. Pincus, M. M. Falinski, W. Shi, P. Coish, D. L. Plata and P. A. Anastas, *Green Chem.*, 2018, **20**, 1929–1961; (*b*) M. Pérez-Venegas and E. Juaristi, *ACS Sustainable Chem. Eng.*, 2020, **8**, 8881–8893; (*c*) H. Mousavi, *Int. J. Bio. Macromol.*, 2021, **186**, 1003–1166; (*d*) M. Rimaz, H. Mousavi, B. Khalili and F. Aali, *J. Chin. Chem. Soc.*, 2018, **65**, 1389–1397; (*e*) M. Rimaz, H. Mousavi, M. Behnam and B. Khalili, *Curr. Chem. Lett.*, 2016, **5**, 145–154; (*f*) M. Rimaz, Z. Jalalian, H. Mousavi and R. H. Prager, *Tetrahedron Lett.*, 2016, **57**, 105–109; (*g*) N. Nivetha and A. Thangamani, *J. Mol. Struct.*, 2021, **1242**, 130716.

2 (*a*) A. Y. Li and A. Moores, *ACS Sustainable Chem. Eng.*, 2019, **7**, 10182–10197; (*b*) G. J. Hutching, *ACS Cent. Sci.*, 2018, **4**, 1095–1101; (*c*) P. T. Anastas, M. M. Kirchhoff and T. C. Williamson, *Appl. Catal., A*, 2001, **221**, 3–13; (*d*) G. Centi and S. Perathoner, *Top. Catal.*, 2009, **52**, 948–961; (*e*) A. C. Lamb, A. F. Lee and K. Wilson, *Aust. J. Chem.*, 2020, **73**, 832–852.

3 (*a*) E. D. Goodman, C. Zhao and M. Cargnello, *ACS Cent. Sci.*, 2020, **6**, 1916–1937; (*b*) R. Schlögl, *Angew. Chem., Int. Ed.*, 2015, **54**, 3465–3520; (*c*) R. Lung, X. Du, Y. Huang, X. Jiang, Q. Zhang, Y. Guo, K. Liu, B. Qiao, A. Wang and T. Zhang,

*Chem. Rev.*, 2020, **120**, 11986–12043; (*d*) R. Lippi, C. J. Coghlan, S. C. Howard, C. D. Easton, Q. Gu, J. Patel, C. J. Sumby, D. F. Kennedy and C. J. Dooman, *Aust. J. Chem.*, 2020, **73**, 1271–1283; (*e*) N. Tadon, S. M. Patil, R. Tadon and P. Kumar, *RSC Adv.*, 2021, **11**, 21291–21300.

4 (*a*) V. Polshetiwar, R. Luque, A. Fihri, H. Zhu, M. Bouhara and J.-M. Basset, *Chem. Rev.*, 2011, **111**, 3036–3075; (*b*) S. Shylesh, V. Schünemann and W. R. Thiel, *Angew. Chem., Int. Ed.*, 2010, **49**, 3428–3459; (*c*) D. Wang and D. Astruc, *Chem. Rev.*, 2014, **114**, 6949–6985; (*d*) M. B. Gawande, R. Luque and R. Zboril, *ChemCatChem*, 2014, **6**, 3312–3313; (*e*) B. Karimi, F. Mansouri and H. M. Mirzaei, *ChemCatChem*, 2015, **7**, 1736–1789; (*f*) G. Mohammadi Ziarani, Z. Kheilkordi, F. Mohajer, A. Badiei and R. Luque, *RSC Adv.*, 2021, **11**, 17456–17477; (*g*) A. Pawar, S. Gajare, A. Patil, R. Kurane, G. Rashinkar and S. Patil, *Res. Chem. Intermed.*, 2021, **47**, 2801–2820; (*h*) M. Aghaei-Hashjin, A. Yahyazadeh and E. Abbaspour-Gilandeh, *RSC Adv.*, 2021, **11**, 23491–23505; (*i*) F. Mohammadsaleh, M. Dehdashti Jahromi, A. R. Hajipour, S. M. Hosseini and K. Niknam, *RSC Adv.*, 2021, **11**, 20812–20823; (*j*) N. Hosseini Mohtasham and M. Gholizadeh, *Res. Chem. Intermed.*, 2021, **47**, 2507–2525.

5 (*a*) A. Maity and V. Polshettiwar, *ChemSusChem*, 2017, **10**, 3866–3913; (*b*) X. Huang, Z. Tao, J. C. Praskavich, A. Goswami, J. F. Al-Sharab, T. Minko, V. Polshettiwar and T. Asefa, *Langmuir*, 2014, **30**, 10886–10898; (*c*) M. Shaban and M. Hasanzadeh, *RSC Adv.*, 2020, **10**, 37116–37133; (*d*) P. Hao, B. Peng, B.-Q. Shan, T.-Q. Yang and K. Zhang, *Nanoscale Adv.*, 2020, **2**, 1792–1810; (*e*) A. Wang, X. Du, Z. Liu, S. Shi and H. Lv, *J. Mater. Chem. A*, 2019, **7**, 5111–5152.

6 V. Polshettiwar, D. Cha, X. Zhang and J. M. Basset, *Angew. Chem., Int. Ed.*, 2010, **49**, 9652–9656.

7 (*a*) A. Hassankhani, S. M. Sadeghzadeh and R. Zhiani, *RSC Adv.*, 2018, **8**, 8761–8769; (*b*) S. M. Sadeghzadeh, *RSC Adv.*, 2016, **6**, 99586–99594; (*c*) A. Allahresani, E. Naghdi, M. A. Nasseri and K. Hemmat, *RSC Adv.*, 2020, **10**, 37974–37981; (*d*) S. M. Sadeghzadeh, *Catal. Sci. Technol.*, 2016, **6**, 1435–1441; (*e*) Z. Dong, G. Yu and X. Le, *New J. Chem.*, 2015, **39**, 8623–8629; (*f*) S. M. Sadeghzadeh, R. Zhiani, S. Emrani and M. Ghabdian, *RSC Adv.*, 2017, **7**, 50838–50843; (*g*) R. Zhiani, S. M. Sadeghzadeh and S. Emrani, *RSC Adv.*, 2018, **8**, 6259–6266; (*h*) M. Dhiman and V. Polshettiwar, *J. Mater. Chem. A*, 2016, **4**, 12416–12424; (*i*) P. Gautam, M. Dhiman, V. Polshettiwar and B. M. Bhanage, *Green Chem.*, 2016, **18**, 5890–5899; (*j*) X. Le, Z. Dong, Y. Liu, Z. Jin, T.-D. Huy, M. Le and J. Ma, *J. Mater. Chem. A*, 2014, **2**, 19696–19706; (*k*) S. M. Sadeghzadeh, *RSC Adv.*, 2016, **6**, 54236–54240; (*l*) S. Azizi and N. Shadjou, *Heliyon*, 2021, **7**, e05915.

8 (*a*) A. Ahmad, S. N. A. Shah, M. Arshad, F. Bélanger-Gariepy, E. R. T. Tiekink and Z. ur Rehman, *Appl. Organomet. Chem.*, 2021, **35**, e6065; (*b*) S. Majhi, K. Sharma, R. Singh, M. Ali, C. S. P. Tripathi and D. Guin, *ChemistrySelect*, 2020, **5**, 12365–12370; (*c*) A. H. T. N. Sorenson, Y. Wu, E. K. Orcutt, R. V. Kent, H. C. Anderson, A. J. Matzger and K. J. Stowers, *J. Mater. Chem. A*, 2020, **8**, 15066–15073; (*d*) B. J. Borah and P. Bharali, *Appl. Organomet. Chem.*, 2020, **34**, e5753; (*e*) N. T. N. Anh and R.-a. Doong, *ACS Appl. Nano Mater.*, 2018, **1**, 2153–2163; (*f*) M. Fu, M. Li, Y. Zhao, Y. Bai, X. Fang, X. Kang, M. Yang, Y. Wei and X. Xu, *RSC Adv.*, 2021, **11**, 26502–26508; (*g*) S. Ansari, A. Khorshidi and S. Shariati, *RSC Adv.*, 2020, **10**, 3554–3565; (*h*) N. Y. Baran, *J. Mol. Struct.*, 2020, **1220**, 128697; (*i*) J. Xiao, Z. Wu, K. Li, Z. Zhao and C. Liu, *RSC Adv.*, 2022, **12**, 1051–1061.

9 (*a*) R. N. Butler and A. C. Coyne, *Chem. Rev.*, 2010, **110**, 6302–6337; (*b*) A. Chanda and V. V. Fokin, *Chem. Rev.*, 2009, **109**, 725–748; (*c*) M. Rimaz, J. Khalafy, H. Mousavi, S. Bohlooli and B. Khalili, *J. Heterocycl. Chem.*, 2017, **54**, 3174–3186; (*d*) M. Rimaz, J. Khalafy and H. Mousavi, *Res. Chem. Intermed.*, 2016, **42**, 8185–8200; (*e*) M. H. Sayahi, S. Bahadorikhalili, S. J. Saghanezhad, M. A. Miller and M. Mahdavi, *Res. Chem. Intermed.*, 2020, **46**, 491–507; (*f*) H. Mousavi, *J. Mol. Struct.*, 2022, **1251**, 131742.

10 (*a*) S. Emami and S. Dadashpour, *Eur. J. Med. Chem.*, 2015, **102**, 611–630; (*b*) L. Zhang and Z. Xu, *Eur. J. Med. Chem.*, 2019, **181**, 111587; (*c*) M. Holiyachi, S. L. Shastri, B. M. Chougala, N. S. Naik, V. Pawar, L. A. Shastri, S. D. Joshi and V. A. Sunagar, *J. Mol. Struct.*, 2021, **1237**, 130424; (*d*) S. Mamidala, V. Vangala, S. R. Peddi, R. Chedupaka, V. Manga and R. R. Vedula, *J. Mol. Struct.*, 2021, **1233**, 130111; (*e*) S. Vaseghi, S. Emami, M. Shokerzadeh, Z. Hossaini and M. Yousefi, *J. Mol. Struct.*, 2021, **1244**, 130926; (*f*) S. Kecel-Gunduz, Y. Budama-Kilinc, B. Gok, B. Bicak, G. Akman, B. Arvas, F. Aydogan and C. Yolacan, *J. Mol. Struct.*, 2021, **1239**, 130539; (*g*) S. T. Bhaskaran and P. Mathew, *J. Mol. Struct.*, 2022, **1251**, 132071; (*h*) X.-F. Song, J. Fan, L. Liu, X.-F. Liu and F. Gao, *Arch. Pharm.*, 2020, **353**, 2000025; (*i*) M. Simic, M. Petkovic, P. Jovanovic, M. Jovanovic, G. Tasic, I. Besu, Z. Zizak, I. Aleksic, J. Nikodinovic-Runic and V. Savic, *Arch. Pharm.*, 2021, **354**, 2100238.

11 (*a*) I. Kostova, S. Bhatia, P. Grigorov, S. Balkansky, V. S. Parmar, A. K. Prasad and L. Saso, *Curr. Med. Chem.*, 2011, **18**, 3929–3951; (*b*) K. O. Lamara, M. Makhloufi-Chebli, A. Benazzouz-Touami, S. Terrachet-Bouaziz, N. Hamid, A. M. S. Silva and J.-B. Behr, *J. Mol. Struct.*, 2021, **1231**, 129936.

12 N. A. Abdel-Latif, *Sci. Pharm.*, 2005, **73**, 193–216.

13 K. Bhagat, J. Bhagat, M. K. Gupta, J. V. Singh, H. K. Gulati, A. Singh, K. Kaur, G. Kaur, S. Sharma, K. Rana, H. Singh, S. Sharma and P. M. Singh Bedi, *ACS Omega*, 2019, **4**, 8720–8730.

14 B. V. Cheriyan, P. Kadhirvelu, J. Nadipelly, J. Shanmugasundaram, V. Sayeli and V. Subramanian, *Pharmacogn. Mag.*, 2017, **13**, 81–84.

15 A. Sánchez-Recillas, G. Navarrete-Vázquez, S. Hidalgo-Figueroa, M. Y. Rios, M. Ibarra-Barajas and S. Estrada-Soto, *Eur. J. Med. Chem.*, 2014, **77**, 400–408.

16 J. Grover and S. M. Jachak, *RSC Adv.*, 2015, **5**, 38892–38905.

17 R. S. Keri, K. M. Hosamani, R. V. Shingalapur and M. H. Hugar, *Eur. J. Med. Chem.*, 2010, **45**, 2597–2605.

18 G. A. Gonçalves, A. R. Spillere, G. M. das Neves, L. P. Kagami, G. L. von Poser, R. F. S. Canto and V. Eifler-Lima, *Eur. J. Med. Chem.*, 2020, **203**, 112514.

19 M. Monti, M. Pinotti, G. Appendino, F. Dallocchino, T. Bellini, F. Antognoni, F. Poli and F. Bernardi, *Biochim. Biophys. Acta, Gen. Subj.*, 2007, **1770**, 1437–1440.
20 D. S. Reddy, M. Kongot and A. Kumar, *Tuberculosis*, 2021, **127**, 102050.
21 M. Z. Hassan, H. Osman, M. A. Ali and M. J. Ashan, *Eur. J. Med. Chem.*, 2016, **123**, 236–255.
22 (*a*) Y. Hu, Y. Shen, X. Wu, X. Tu and G.-X. Wang, *Eur. J. Med. Chem.*, 2018, **143**, 958–969; (*b*) C. R. Sahoo, J. Sahoo, M. Mahapatra, D. Lenka, P. K. Sahu, B. Dehury, R. N. Padhy and S. K. Paidesetty, *Arabian J. Chem.*, 2021, **14**, 102922; (*c*) D. Feng, A. Zhang, Y. Yang and P. Yang, *Arch. Pharm.*, 2020, **353**, 1900380.
23 R. Elias, R. I. Benhamou, Q. Z. Jaber, O. Dorot, S. L. Zada, K. Oved, E. Pichinuk and M. Fridman, *Eur. J. Med. Chem.*, 2019, **179**, 779–790.
24 K. V. Sashidhara, A. Kumar, R. P. Dodda, N. N. Krishna, P. Agarwal, K. Srivastava and S. K. Puri, *Bioorg. Med. Chem. Lett.*, 2012, **22**, 3926–3930.
25 H. Li, Y. Yao and L. Li, *J. Pharm. Pharmacol.*, 2017, **69**, 1253–1264.
26 (*a*) J. Neyts, E. De Clercq, R. Singha, Y. H. Chang, A. R. Das, S. K. Chakraborty, S. C. Hong, S.-C. Tsay, M.-H. Hsu and J. R. Hwu, *J. Med. Chem.*, 2009, **52**, 1486–1490; (*b*) J. R. Hwu, S.-Y. Lin, S.-C. Tsay, E. De Clercq, P. Leyssen and J. Neyts, *J. Med. Chem.*, 2011, **54**, 2114–2126.
27 Z. Xu, Q. Chen, Y. Zhang and C. Liang, *Fitoterapia*, 2021, **150**, 104863.
28 S. García, I. Mercado-Sánchez, L. Bahena, Y. Alcaraz, M. A. García-Revilla, J. Robles, N. Santos-Martínez, D. Ordaz-Rosado, R. García-Becerra and M. A. Vazquez, *Molecules*, 2020, **25**, 5134.
29 C. Zaragozá, F. Zaragozá, I. Gayo-Abeleira and L. Villaescusa, *Molecules*, 2021, **26**, 3036.
30 N. Yadav, D. Agarwal, S. Kumar, A. K. Dixit, R. D. Gupta and S. K. Awasthi, *Eur. J. Med. Chem.*, 2018, **145**, 735–745.
31 F. Yilmaz, E. Menteşe and B. B. Sökmen, *J. Heterocycl. Chem.*, 2021, **58**, 260–269.
32 (*a*) P. Anand, B. Singh and N. Singh, *Bioorg. Med. Chem.*, 2012, **20**, 1175–1180; (*b*) M.-q. Song, W. Min, J. Wang, X.-X. Si, X.-J. Wang, Y.-W. Liu and D.-H. Shi, *J. Mol. Struct.*, 2021, **1229**, 129784; (*c*) A. Benazzouz-Touami, A. Chouh, S. Halit, S. Terrachet-Bouaziz, M. Makhloufi-Chebli, K. Ighil-Ahriz and A. M. S. Silve, *J. Mol. Struct.*, 2022, **1249**, 131591.
33 (*a*) H. M. Revankar, S. N. A. Bukhari, G. B. Kumar and H.-L. Qin, *Bioorg. Chem.*, 2017, **71**, 146–159; (*b*) D. AL-Duhaidahawi, H. F. S. AL-Zubaidy, K. Al-Khafaji and A. Al-Amiery, *J. Mol. Struct.*, 2022, **1247**, 131377.
34 M. Roussaki, K. Zelianaios, E. Kavetsou, S. Hamilakis, D. Hadjipavlou-Litina, C. Kontogiorgis, T. Liargkova and A. Detsi, *Bioorg. Med. Chem.*, 2014, **22**, 6586–6594.
35 F. Chimenti, D. Secci, A. Bolasco, P. Chimenti, B. Bizzarri, A. Granese, S. Carradori, M. Yáñez, F. Orallo, F. Ortuso and S. Alcaro, *J. Med. Chem.*, 2009, **52**, 1935–1942.
36 D. Cao, Y. Liu, W. Yan, C. Wang, P. Bai, T. Wang, M. Tang, X. Wang, Z. Yang, B. Ma, L. Ma, L. Lei, F. Wang, B. Xu, Y. Zhou, T. Yang and L. Chen, *J. Med. Chem.*, 2016, **59**, 5721–5739.
37 M. Bozdag, M. Ferraroni, F. Carta, D. Vullo, L. Lucarini, E. Orlandini, A. Rossello, E. Nuti, A. Scozzafava, E. Masini and C. T. Supuran, *J. Med. Chem.*, 2014, **57**, 9152–9167.
38 (*a*) Q. Shen, J. Shao, Q. Peng, W. Zhang, L. Ma, A. S. C. Chan and L. Gu, *J. Med. Chem.*, 2010, **53**, 8252–8259; (*b*) X.-T. Xu, X.-Y. Deng, J. Chen, Q.-M. Liang, K. Zhang, D.-L. Li, P.-P. Wu, X. Zheng, R.-P. Zhou, Z.-Y. Jiang, A.-J. Ma, W.-H. Chen and S.-H. Wang, *Eur. J. Med. Chem.*, 2020, **189**, 112013; (*c*) S. Ansari, H. Azizian, K. Pedrood, A. Yavari, S. Mojtabavi, M. A. Faramarzi, S. Golshani, S. Hosseini, M. Biglar, B. Larijani, H. Rastegar, H. Hamedifar, M. Mohammadi-Khanaposhtani and M. Mahdavi, *Arch. Pharm.*, 2021, **354**, 2100179.
39 S. Ranatunga, C.-H. A. Tang, C. W. Kang, C. L. Kriss, B. J. Kloppenburg, C.-C. A. Hu and J. R. Del Valle, *J. Med. Chem.*, 2014, **57**, 4289–4301.
40 G. Cai, W. Yu, D. Song, W. Zhang, J. Guo, J. Zhu, Y. Ren and L. Kong, *Eur. J. Med. Chem.*, 2019, **174**, 236–251.
41 J. Xu, H. Li, X. Wang, J. Huang, S. Li, C. Liu, R. Dong, G. Zhu, C. Duan, F. Jiang, Y. Zhang, Y. Zhu, T. Zhang, Y. Chen, W. Tang and T. Lu, *Eur. J. Med. Chem.*, 2020, **200**, 112424.
42 D. Liang, Y. Fan, Z. Yang, Z. Zhang, M. Liu, L. Liu and C. Jiang, *Eur. J. Med. Chem.*, 2020, **187**, 111923.
43 C. Bouckaert, S. Serra, G. Rondelet, E. Dolušić, J. Wouters, J.-M. Dogné, R. Frédérick and L. Pochet, *Eur. J. Med. Chem.*, 2016, **110**, 181–194.
44 A. Chilin, R. Battistutta, A. Bortolato, G. Cozza, S. Zanatta, G. Poletto, M. Mazzorana, G. Zagotto, E. Uriarte, A. Guiotto, L. A. Pinna, F. Meggio and S. Moro, *J. Med. Chem.*, 2008, **51**, 752–759.
45 M. Daśko, M. Przybyłowska, J. Rachon, M. Masłyk, K. Kubiński, M. Misiak and A. Składnowska, *Eur. J. Med. Chem.*, 2017, **128**, 79–87.
46 Q. Ji, Z. Ge, Z. Ge, K. Chen, H. Wu, X. Liu, Y. Huang, Y. Lvjiang, X. Yang and F. Liao, *Eur. J. Med. Chem.*, 2016, **108**, 166–176.
47 G. Li, D. Wang, M. Sun, G. Li, J. Hu, Y. Zhang, Y. Yuan, H. Ji, N. Chen and G. Liu, *J. Med. Chem.*, 2010, **53**, 1741–1754.
48 (*a*) H. Deng, H. Hu, M. He, J. Hu, W. Niu, A. M. Ferrie and Y. Fang, *J. Med. Chem.*, 2011, **54**, 7385–7396; (*b*) L. Wei, T. Hou, J. Li, X. Zhang, H. Zhou, Z. Wang, J. Cheng, K. Xiang, J. Wang, Y. Zhao and X. Liang, *J. Med. Chem.*, 2021, **64**, 2634–2647.
49 V. Rempel, N. Volz, F. Gläser, M. Nieger, S. Bräse and C. E. Müller, *J. Med. Chem.*, 2013, **56**, 4798–4810.
50 M. J. Matos, S. Vilar, S. Vasquez-Rodriguez, S. Kachler, K.-N. Klotz, M. Buccioni, G. Delogu, L. Santana, E. Uriarte and F. Borges, *J. Med. Chem.*, 2020, **63**, 2577–2587.
51 (*a*) A. Dömling, W. Wang and K. Wang, *Chem. Rev.*, 2012, **112**, 3083–3135; (*b*) S. Abu-Melha, Z. A. Muhammad, A. S. Abouzid, M. M. Edrees, A. S. Abo Dena, S. Nabil and S. M. Gomha, *J. Mol. Struct.*, 2021, **1234**, 130180; (*c*) H. G. O. Alvim, E. N. da Silva Júnior and B. A. D. Neto, *RSC Adv.*, 2014, **4**, 54282–54299; (*d*) S. Kamalifar and H. Kiyani, *Res. Chem. Intermed.*, 2019, **45**, 5975–5987; (*e*) L. Wu,

S. Yan, W. Wang and Y. Li, *Res. Chem. Intermed.*, 2020, **46**, 4311–4322; (*f*) A. Patil, S. Shinde, G. Rashinkar and R. Salunkhe, *Res. Chem. Intermed.*, 2020, **46**, 63–73; (*g*) S. Zhi, X. Ma and W. Zhang, *Org. Biomol. Chem.*, 2019, **17**, 7632–7650; (*h*) N. Nikooei, M. G. Dekamin and E. Valiey, *Res. Chem. Intermed.*, 2020, **46**, 3891–3909; (*i*) M. Rimaz and H. Mousavi, *Turk. J. Chem.*, 2013, **37**, 252–261; (*j*) M. Rimaz, H. Mousavi, L. Ozzar and B. Khalili, *Res. Chem. Intermed.*, 2019, **45**, 2673–2694; (*k*) M. Rimaz, H. Mousavi, B. Khalili and L. Sarvari, *J. Iran. Chem. Soc.*, 2019, **16**, 1687–1701; (*l*) M. Rimaz, B. Khalili, G. Khatyal, H. Mousavi and F. Aali, *Aust. J. Chem.*, 2017, **70**, 1274–1284; (*m*) M. Rimaz, H. Mousavi, M. Behnam, L. Sarvari and B. Khalili, *Curr. Chem. Lett.*, 2017, **6**, 55–68; (*n*) M. Rimaz, H. Mousavi, L. Nikpey and B. Khalili, *Res. Chem. Intermed.*, 2017, **43**, 3925–3937; (*o*) M. Rimaz, H. Mousavi, P. Keshavarz and B. Khalili, *Curr. Chem. Lett.*, 2015, **4**, 159–168; (*p*) P. Mane, B. Shinde, P. Mundada, B. Karale and A. Burungale, *Res. Chem. Intermed.*, 2021, **47**, 1743–1758; (*q*) I. Yellapurkar, S. Bhabal, M. M. V. Ramana, K. Jangam, V. Salve, S. Patange and P. More, *Res. Chem. Intermed.*, 2021, **47**, 2669–2687; (*r*) R. L. Mohlala, E. M. Coyanis, M. A. Fernandes and M. L. Bode, *RSC Adv.*, 2021, **11**, 24466–24473; (*s*) F. Haji Norouzi, N. Foroughifar, A. Khajeh-Amiri and H. Pasdar, *RSC Adv.*, 2021, **11**, 29948–29959; (*t*) B. M. Bizzarri, A. Fanelli, L. Botta, M. De Angelis, A. T. Palamara, L. Nencioni and R. Saladino, *RSC Adv.*, 2021, **11**, 30020–30029; (*u*) Z. Ghanbari and H. Naeimi, *RSC Adv.*, 2021, **11**, 31377–31384; (*v*) P. Ghamari Kargar, G. Bagherzade and H. Eshghi, *RSC Adv.*, 2021, **11**, 4339–4355; (*w*) P. Ghamari Kargar and G. Bagherzade, *RSC Adv.*, 2021, **11**, 23192–23206; (*x*) P. Ghamari Kargar, M. Noorian, E. Chamani, G. Bagherzade and Z. Kiani, *RSC Adv.*, 2021, **11**, 17413–17430; (*y*) S. Khajeh Dangolian, E. Niknam, O. Shahraki and A. Khalafi-Nezhad, *J. Mol. Struct.*, 2021, **1245**, 131061; (*z*) F. Kamali and F. Shirini, *J. Mol. Struct.*, 2021, **1227**, 129654.

52 (*a*) H. Mousavi, B. Zeynizadeh, R. Younesi and M. Esmati, *Aust. J. Chem.*, 2018, **71**, 595–660; (*b*) B. Zeynizadeh, R. Younesi and H. Mousavi, *Res. Chem. Intermed.*, 2018, **44**, 7331–7352; (*c*) B. Zeynizadeh, F. Mohammad Aminzadeh and H. Mousavi, *Res. Chem. Intermed.*, 2019, **45**, 3329–3357; (*d*) B. Zeynizadeh, H. Mousavi and S. Zarrin, *J. Chin. Chem. Soc.*, 2019, **66**, 928–933; (*e*) B. Zeynizadeh, F. Mohammad Aminzadeh and H. Mousavi, *Green Process. Synth.*, 2019, **8**, 742–755; (*f*) B. Zeynizadeh, F. Sepehraddin and H. Mousavi, *Ind. Eng. Chem. Res.*, 2019, **58**, 16379–16388; (*g*) R. Bakhshi, B. Zeinizadeh and H. Mousavi, *J. Chin. Chem. Soc.*, 2020, **67**, 623–637; (*h*) B. Zeynizadeh, H. Mousavi and F. Sepehraddin, *Res. Chem. Intermed.*, 2020, **46**, 3361–3382; (*i*) B. Zeynizadeh, F. Mohammad Aminzadeh and H. Mousavi, *Res. Chem. Intermed.*, 2021, **47**, 3289–3312; (*j*) B. Zeynizadeh, H. Mousavi and F. Mohammad Aminzadeh, *J. Mol. Struct.*, 2022, **1255**, 131926.

53 X. Li, W. She, J. Wang, W. Li and G. Li, *Appl. Organomet. Chem.*, 2021, **35**, e6294.

54 J. Shabir, C. Garkoti, P. Gupta, M. Sharma, S. Rani, M. Kumari and S. Mozumdar, *ACS Omega*, 2021, **6**, 1415–1425.

55 C. Sharma, A. K. Srivastava, A. Soni, S. Kumari and R. K. Joshi, *RSC Adv.*, 2020, **10**, 32516–32521.

56 J. Du, J. Chen, H. Xia, Y. Zhao, F. Wang, H. Liu, W. Zhou and B. Wang, *ChemCatChem*, 2020, **12**, 2426–2430.

57 M. Gholinejad, E. Oftadeh, M. Shojafar, J. M. sansano and B. H. Lipshutz, *ChemSusChem*, 2019, **12**, 4240–4248.

58 V. S. Sypu, M. Bhaumik, K. Raju and A. Maity, *J. Colloid Interface Sci.*, 2021, **581**, 979–989.

59 Y. Li, W. Jiang, G. Ma and M. M. Zanganeh, *Int. J. Bio. Macromol.*, 2020, **163**, 2162–2171.

60 M. Kaur, C. Sharma, N. Sharma, B. Jawal and S. Paul, *ACS Appl. Nano Mater.*, 2020, **3**, 10310–10325.

61 S. Yang, Z.-H. Zhang, Q. Chen, M.-Y. He and L. Wang, *Appl. Organomet. Chem.*, 2018, **32**, e4132.

62 F. M. Moghaddam, V. Saberi and P. Kalvani, *ChemistrySelect*, 2018, **3**, 6779–6785.

63 M. Pashaei and E. Mehdipour, *Appl. Organomet. Chem.*, 2018, **32**, e4226.

64 B. Zeynizadeh, S. Rahmani and H. Tizhoush, *Polyhedron*, 2020, **175**, 114201.

65 M. Gilanizadeh and B. Zeynizadeh, *J. Iran. Chem. Soc.*, 2018, **15**, 2831–2837.

66 M. Piri, M. M. Heravi, A. Elhampour and F. Nemati, *J. Mol. Struct.*, 2021, **1242**, 130646.

67 Z. Shokri, B. Zeynizadeh and S. A. Hosseini, *J. Colloid Interface Sci.*, 2017, **485**, 99–105.

68 V. Bilakanti, N. Gutta, V. K. Velisoju, M. Dumpalapally, S. Inkollu, N. Nama and V. Akula, *React. Kinet., Mech. Catal.*, 2020, **130**, 347–362.

69 B. Zeynizadeh, Z. Shokri and I. Mohammadzadeh, *J. Iran. Chem. Soc.*, 2020, **17**, 859–870.

70 B. Akhlaghinia, P. Sanati, A. Mohammadinezhad and Z. Zarei, *Res. Chem. Intermed.*, 2019, **45**, 3215–3235.

71 C. Patil, S. K. Shinde, U. P. Patil, A. T. Birajdar and S. S. A. Patil, *Res. Chem. Intermed.*, 2021, **47**, 1675–1691.

72 S. Rahmani and B. Zeynizadeh, *Res. Chem. Intermed.*, 2019, **45**, 1227–1248.

73 D. K. Agarwal, A. Sethiya, P. Teli, A. Manhas, J. Sani, N. Sahiba, P. C. Jha, S. Agarwal and P. K. Goyal, *J. Heterocycl. Chem.*, 2020, **57**, 3294–3309.

74 F. Shirini, A. Fallah-Shojaei, L. Samavi and M. A. Abedini, *RSC Adv.*, 2016, **6**, 48469–48478.

75 M. Seddighi, F. Shirini and M. Mamaghani, *RSC Adv.*, 2013, **3**, 24046–24053.

76 X. Wu and W.-X. Peng, *J. Chin. Chem. Soc.*, 2020, **67**, 2129–2148.

77 N. O. Mahmoodi, Z. Jalalifard and G. Pirbasti Fathanbari, *J. Chin. Chem. Soc.*, 2020, **67**, 172–182.

78 R. Teimuri-Mofrad, S. Tahmasebi and E. Payami, *Appl. Organomet. Chem.*, 2019, **33**, e4773.

79 S. Mathavan, K. Kannan and R. B. R. D. Yamajala, *Org. Biomol. Chem.*, 2019, **17**, 9620–9626.

80 E. El hajri, Z. Benzekri, S. Sibous, A. Ouasri, S. Boukhris, A. Hassikou, A. Rhandour and A. Souizi, *J. Mol. Struct.*, 2021, **1230**, 129890.

81 R. Pourhasan-Kisomi, F. Shirini and M. Golshekan, *Appl. Organomet. Chem.*, 2018, **32**, e4371.
82 M. Ziyaadini, N. Nemat-Bakhsh, S. J. Roudbaraki and M. Ghashang, *Polycyclic Aromat. Compd.*, 2022, **42**, 460–474.
83 M. M. Khodaei, A. Alizadeh and M. A. Haghipour, *Res. Chem. Intermed.*, 2020, **46**, 1033–1045.
84 S. Abdolahi, M. Hajjami and F. Gholamian, *Res. Chem. Intermed.*, 2021, **47**, 1883–1904.
85 S. Amirnejat, A. Nosrati, R. Peymanfar and S. Javanshir, *Res. Chem. Intermed.*, 2020, **46**, 3683–3701.
86 H. Foroughi Niya, N. Hazeri, M. Rezaie Kahkhaie and M. T. Maghsoodlou, *Res. Chem. Intermed.*, 2020, **46**, 1685–1704.
87 F. Hasaanzadeh, N. Daneshvar, F. Shirini and M. Mamaghani, *Res. Chem. Intermed.*, 2020, **46**, 4971–4984.
88 A. Mahajan and M. Gupta, *Appl. Organomet. Chem.*, 2021, **35**, e6161.
89 P. Mohammadi and H. Sheibani, *Mater. Chem. Phys.*, 2019, **228**, 140–146.
90 M. Khaleghi Abbasabadi, D. Azarifar and H. R. Esmaili Zand, *Appl. Organomet. Chem.*, 2020, **34**, e6004.